# Implementation of an iterative matching scheme for the Kapchinskij-Vladimirskij equations in the WARP code

by

Sven H. Chilton

S.B. (Massachusetts Institute of Technology) 2005

A thesis submitted in partial satisfaction of the
requirements for the degree of
Master of Science

in

Nuclear Engineering

in the

GRADUATE DIVISION
of the
UNIVERSITY OF CALIFORNIA, BERKELEY

Committee in charge:
Professor John Verboncoeur, Chair
Professor Edward Morse
Doctor Steven Lund

Spring 2008

The dissertation of Sven H. Chilton is approved:

_____

Chair                                                                              Date

_____

Date

_____

Date

University of California, Berkeley

Spring 2008

# Abstract

Implementation of an iterative matching scheme for the Kapchinskij-Vladimirskij equations in the WARP code

by

Sven H. Chilton

Master of Science in Nuclear Engineering

University of California, Berkeley

Professor John Verboncoeur, Chair

The WARP code is a robust electrostatic particle-in-cell simulation package used to model charged particle beams with strong space-charge forces. A fundamental operation associated with seeding detailed simulations of a beam transport channel is to generate initial conditions where the beam distribution is matched to the structure of a periodic focusing lattice. This is done by solving for periodic, matched solutions to a coupled set of ODEs called the Kapchinskij-Vladimirskij (KV) envelope equations, which describe the evolution of low-order beam moments subject to applied lattice focusing, space-charge defocusing, and thermal defocusing forces. Recently, an iterative numerical method was developed (Lund, Chilton, and Lee, *Efficient computation of matched solutions to the KV envelope equations for periodic focusing lattices*, Physical Review Special Topics – Accelerators and Beams **9**, 064201 2006) to generate matching conditions in a highly flexible, convergent, and fail-safe

manner. This method is extended and implemented in the WARP code as a Python package to vastly ease the setup of detailed simulations. In particular, the Python package accommodates any linear applied lattice focusing functions without skew coupling, and a more general set of beam parameter specifications than its predecessor. Lattice strength iteration tools were added to facilitate the implementation of problems with specific applied focusing strengths.

Professor John Verboncoeur
Dissertation Committee Chair

För kärlek, i framtiden

# Contents

# List of Figures

# List of Tables

## Acknowledgments

# Chapter 1

# Introduction

## 1.1 Motivation

The Heavy Ion Fusion Science Virtual National Laboratory (HIFS-VNL) carries out research on warm dense matter physics and developing heavy ion driven energy production via inertial confinement fusion. A heavy ion accelerator-based driver is envisioned to consist of one or more linear accelerators focusing ion beams propagating toward a targeting chamber. Inertial fusion devices have been designed with as few as 8 beams and as many as hundreds. In the so-called final focusing region, the beams are focused tightly onto the target, with a spot size of ~2 mm (diameter). At the center of the targeting chamber is a spherical capsule of fuel, typically a deuterium-tritium mixture, usually encased in a thin plastic shell. Beam energy incident on the capsule is then absorbed in the outer layer of the pellet, causing the plastic coating to ablate in rocket-like blowoff. This ablation compresses the fuel, increasing its density and pressure, facilitating nuclear fusion. Fuel temperature also increases during the compression. Ideally, the fuel temperature should be

higher than the Coulomb barrier (which inhibits fusion reactions) but not so high that the fusion cross-section of the fuel is lowered.

A fusion capsule can be driven either directly or indirectly. In a direct drive, the beams deposit energy in the target directly, while in an indirect drive, the beams deposit energy onto an intermediate called a hohlraum. When beams are absorbed in the walls of a hohlraum, the deposited kinetic energy heats the walls, which then radiate x-rays. The hohlraum's internal geometry is tuned such that the x-rays deposit energy on the capsule as uniformly as possible. The x-rays are emitted and absorbed many times, which aids this smoothing.

Direct drive has an advantage over indirect drive in that a greater fraction of the beam energy can be imparted onto the target by eliminating the larger hohlraum volume needing to be heated in indirect drive. However, it is considerably more difficult to ensure that the target is radiated uniformly with direct drive composed of a limited number of beams. Non-uniformities in heating can lead to less efficient target compression, premature fuel mixing, and even ejection of fuel.

Inertial confinement devices to date (such as NIF, the National Ignition Facility at Lawrence Livermore National Laboratory) employ lasers as a driver. Three types of lasers are presently under consideration for driving fusion reactions: glass, diode-pumped solid state, and KrF. Using ion beams for this purpose presents several clear advantages for a practical power plant. Glass lasers are limited in their repetition rate because the lasing material must cool down between each pulse. Diode-pumped solid state lasers of the necessary power are prohibitively expensive. KrF lasers have much shorter system

lifetimes than either glass or diode lasers. Moreover, ion beams are expected to make more efficient drivers than lasers. That is, the ratio of energy imparted onto the target to the energy required to create the driving beam is much greater for ion beams than lasers. In terms of heating targets, laser drives typically have an efficiency between 10 and 20% [1], while heavy ion drives have a corresponding efficiency between 25 and 35%. This greater efficiency helps drive down the cost of electricity (COE) for a heavy ion fusion system. According to Ref. [2], a prototype 1GW heavy ion fusion power plant would have a COE of 7.18 cents/kWeh, while Ref. [1] implies a comparable cost for a laser-driven power plant. However, several figures in Ref. [1] seem to indicate that for driver energies and pulse rates equal to those in Ref. [2], a laser drive would have a much higher COE than a heavy ion drive.

Ions can be focused with electromagnetic fields in vacuum rather than with material lenses. Energy imparted into a material lens can damage the optics over many shots and destroy an expensive and complex system component. The fact that ion beams need not touch the elements focusing them allows for high beam repetition rates that could destroy material lenses over many shots. As such, heavy ion fusion drivers are expected to have a much longer lifetime than an equivalent laser-driven system. Perhaps most importantly, the final focusing elements in a heavy ion fusion device do not lie in the beam path, and are thus easier to protect from debris from the target implosions, neutrons, and gamma rays. Typically, a thick liquid shield (in some designs Flibe) encases the targeting chamber, protecting the final focusing elements and allowing for tritium breeding.

Computer-based numerical modeling of charged particle beams subject to both

applied focusing forces and self-generated defocusing forces is essential to designing a heavy ion driver. Given the typical situation of a periodic focusing system and a charged particle beam much longer than the focusing period length, the Kapchinskij-Vladimirskij (KV) envelope equations describe, to low order, the statistical evolution of the transverse beam edge radii. So-called matched solutions to the KV equations have the same period length as the focusing system. Matched beams are believed to be the most radially compact solutions to the KV equations. Thus, beam matching is of fundamental importance in efficient accelerator design. Constructing matched envelope solutions to the KV equations is also a fundamental step in setting up more detailed simulations to verify machine performance.

Focusing ion beams presents a significant challenge. Space-charge and emittance (transverse phase space area) both act to defocus the beam. Beams used in an HIF driver are typically strongly space-charge dominated. To see why, consider a typical driver pulse with an ion kinetic energy of 4.0 GeV, a total energy of 3.61 MJ, and a pulse duration of 9.3 ns (see Sec. II and Table I of Ref. [2]). This pulse is divided over 48 beams composed of singly charged $^{197}$Au ions in a characteristic design choice. This implies that the each individual beam has a value of dimensionless perveance $Q = 7.1 \times 10^{-5}$ [see Eq. (2.13)]. For comparison, consider the Tevatron accelerator at the Fermi National Laboratory. The Tevatron accelerates bunches with $\sim 10^{12}$ protons to a kinetic energy of 1 TeV, with a bunch length of approximately 10 ns. This implies a maximum value $Q = 8.3 \times 10^{-16}$. Since the perveance of a beam characteristic of heavy ion fusion drives is orders of magnitude greater than that of charged particle beams in more conventional accelerators, any beam model applicable to heavy ion fusion must include strong space-charge effects.

Traditional schemes for computing matched beams employ root finding algorithms to determine the initial beam radii and angles necessary to ensure a match [3, 4, 5]. An optimal formulation of the conventional root finding procedure for envelope matching has been presented by Ryne [4]. Typical root finding procedures for matching can be surprisingly problematic even for relatively simple focusing lattices. Variations in initial conditions can lead to many inflection points in the envelope functions at the end of the lattice period. Thus initial guesses close to the actual values corresponding to the periodic solution are often necessary to employ standard root finding techniques. This is especially true for complicated focusing lattices with low degrees of symmetry and where focusing strengths (or equivalently, undepressed single particle phase advances) are large. For large focusing strength and strong space-charge intensity, the matched envelope solution can be unstable over a wide range of system parameters [3, 5]. Such instabilities can restrict the basin of attraction when standard numerical root finding methods are used to calculate the needed matching conditions — especially for certain classes of solution parameterizations.

In this report we present an iterative procedure first discussed in Ref. [6] to numerically calculate matched envelope solutions of the KV equations. The method is implemented in WARP, a large, multidimensional particle-in-cell (PIC) code that serves as the primary simulation code for the HIFS-VNL. The method has also been extended to support a broader class of focusing systems.

The basis of our iterative matching procedure is that the distribution of particle orbits internal to the beam must have a locus of turning points consistent with the beam edge (envelope). In the absence of beam space-charge, particle oscillation (betatron) ampli-

tudes calculated from the sine- and cosine-like principal orbits describing particles moving in the applied focusing fields of the lattice directly specify the matched beam envelope [7]. For finite beam space-charge, the principal orbits and the matched beam envelope cannot be calculated *a priori* because the defocusing forces from beam space-charge uniformly distributed within the (undetermined) beam envelope are unknown. In the iterative matching (IM) method, a relation between the particle orbits in the presence of space-charge and the beam envelope is viewed as a consistency equation. This consistency constraint can be viewed as an expression of a Courant-Snyder invariant [6, 8]. Starting from a simple trial envelope solution that accounts for both space-charge and applied focusing forces in a general manner, the consistency condition is used to iteratively correct the envelope functions until converged matched envelope solutions are obtained that are consistent with particle orbits internal to the beam.

The IM method offers superior performance and reliability in constructing matched envelopes over conventional root finding because the IM iterations are structured to reflect the periodicity of the actual matched solution rather than searching for parameters that lead to periodicity. The IM method works for all physically achievable system parameters (even in cases of envelope instability) and is most naturally expressed and rapidly convergent when the relative beam space-charge strength is expressed in terms of the depressed particle phase advance. All other parameterizations of solutions (specified perveances and emittances, etc.) can be carried out by simple extensions of the IM method rendering the approach fully general. The natural depressed phase advance parameterization is also useful when carrying out parametric studies because phase advances are the most relevant parameters for

analysis of resonance-like effects central to charged particle dynamics in accelerators. The IM method provides a complement to recent analytical perturbation theories developed to construct matched beam envelopes in lattices with certain classes of symmetries [9, 10, 11]. In contrast to these analytical theories, the IM method can be applied to arbitrary linear focusing lattices without skew coupling (i.e. x-y coupling in the linear applied focusing forces). The highly convergent iterative corrections of the IM method have the same form for all order iterations after seeding, rendering the method straightforward to code and apply to numerically generate accurate matched envelope solutions.

In some applications, it is helpful to specify properties of the focusing lattice other than the maximum focusing strength. The undepressed particle phase advance gives the phase change over one lattice period of a single particle subject only to applied focusing fields. A package has been added to allow users to specify a desired undepressed phase advance for a focusing lattice with a given shape. The package calculates the scale factor by which the original lattice focusing function must be multiplied to achieve the desired phase advance. This facility helps code users explore parametric transport limits which are often expressed in terms of phase advances.

## 1.2   WARP

WARP is an electrostatic, multidimensional PIC code developed to model ion beams with intense space-charge for applications to heavy ion fusion [12, 13, 14]. The code contains a versatile set of tools, including particle-moving, field-solving, loading, and diagnostic routines. These are linked by an interactive Python interpreter to allow users to

employ them in a wide variety of simulations without altering the source code. The code includes optimized relativistic and nonrelativistic particle movers and has 2D transverse slice, r-z, and full 3D beam descriptions. Particles are moved synchronously in time in all cases.

WARP is implemented in Fortran 90 (for compiled code; see Ref. [15]) and Python (see Refs. [16, 17]). The Python interface is employed to link Fortran routines to code less numerically intensive operations, such as diagnostics. It also grants the user flexibility to guide simulations. The Fortran routines carry out intense numerical work. A linkage program called Forthon (see Ref. [18]) allows a Python interpreter to access functions defined and quantities calculated in the Fortran routines.

WARP can use matched beams to seed more detailed beam simulations. In the past, WARP has employed root finding algorithms via external packages to calculate initial conditions necessary for matched beams. As discussed previously, such methods can prove problematic. Moreover, these matching methods were only implemented for a few specific, simple lattice types in WARP.

In this study we present the following improvements to WARP: the implementation of a more powerful iterative matching scheme for the KV envelope equations, and the addition of a package allowing users to scale lattice focusing strengths to obtain desired undepressed phase advances.

# Chapter 2

# Theoretical Model

In this chapter we examine the transverse dynamics of charged particle beams subject to applied linear focusing forces. In Sec. 2.1, we derive a model in terms of first and second-order beam moments of the beam distribution function. This model is sufficiently general to allow for lattice skew coupling. In Sec. 2.2, we neglect skew coupling and derive the standard KV envelope equations.

## 2.1 Moment Advance

We consider an unbunched beam containing a single ion species with charge $q$ and mass $m$. We denote the axial coordinate $s$ and the transverse/particle coordinates $x$ and $y$. We assume that the beam propagates with axial relativistic factors $\beta_b = v_b/c$ and $\gamma_b = 1/\sqrt{1 - \beta_b^2}$ in the lab frame, with $v_b$ allowed to vary in $s$. In general, external focusing elements acting on the beam will not be perfectly aligned with the lab coordinate system. Assuming that a focusing element is rotated by an angle $\theta$ with respect to the $x$-axis, we

find that the coordinates in the lens frame (indicated by subscript $l$) are related to the lab

coordinates (no subscript) as follows (see Ref. [19]):

$$x = x_l \cos\theta - y_l \sin\theta \ ; \quad y = x_l \sin\theta + y_l \cos\theta. \tag{2.1}$$

$\theta$ can assume a different value in each optical element, but within each optical element, $\theta$

is constant.

In the lens frame, the applied focusing effects decouple and the particle equations

of motion are given by

$$
\begin{aligned}
x_l''(s) + \frac{(\gamma_b \beta_b)'}{\gamma_b \beta_b} x_l'(s) + \kappa_x(s) x_l(s) &= -\frac{q}{m\gamma_b^3 \beta_b^2 c^2} \frac{\partial\phi}{\partial x_l}, \\
y_l''(s) + \frac{(\gamma_b \beta_b)'}{\gamma_b \beta_b} y_l'(s) + \kappa_y(s) y_l(s) &= -\frac{q}{m\gamma_b^3 \beta_b^2 c^2} \frac{\partial\phi}{\partial y_l}.
\end{aligned}
\tag{2.2}
$$

Here, primes denote derivatives with respect to the axial machine coordinate $s$, the functions

$\kappa_x(s)$ and $\kappa_y(s)$ represent linear applied focusing forces of the transport lattice, $c$ is the speed

of light *in vacuo*, and $\phi$ is the electrostatic potential of the beam. Equations relating the $\kappa$

functions to magnetic and/or electric fields of practical focusing elements are presented in

Ref. [5].

For a general quantity $\zeta$, $\langle\zeta\rangle$ denotes the transverse statistical average of $\zeta$ with

respect to the beam distribution function, i.e.

$$\langle\zeta\rangle \equiv \frac{\int \zeta f(x, y, x', y', s)\, dx\, dy\, dx'\, dy'}{\int f(x, y, x', y', s)\, dx\, dy\, dx'\, dy'}. \tag{2.3}$$

Here, $f$ denotes the ion distribution function and the integrals are evaluated over the entire

transverse phase space. $\langle x\rangle$ and $\langle y\rangle$ represent the transverse beam centroid coordinates.

We assume that the beam has a uniform density elliptical profile centered at the

beam centroid and rotated at some angle $\alpha$ (which can vary in $s$) with respect to the lab

frame. The relationship between the coordinates in the rotated beam frame (indicated by subscript b) and the lab frame is given by:

$$x - \langle x \rangle = x_b \cos \alpha - y_b \sin \alpha \; ; \quad y - \langle y \rangle = x_b \sin \alpha + y_b \cos \alpha. \tag{2.4}$$

Neglecting image charge effects, the electrostatic potential within the beam is

$$\phi(x_b, y_b) = -\frac{\lambda}{2\pi\epsilon_0} \left[ \frac{x_b^2}{(r_x + r_y)r_x} + \frac{y_b^2}{(r_x + r_y)r_y} \right] + \text{const.} \tag{2.5}$$

Here, $\epsilon_0$ is the permittivity of free space and $\lambda$ is the beam's line charge. The beam's semi-axial widths $r_x$ and $r_y$ are related to transverse beam moments as follows:

$$\frac{r_x^2}{4} = \langle x_b^2 \rangle = \left( \langle x^2 \rangle - \langle x \rangle^2 \right) \cos^2 \alpha + \left( \langle y^2 \rangle - \langle y \rangle^2 \right) \sin^2 \alpha + 2 \left( \langle xy \rangle - \langle x \rangle \langle y \rangle \right) \sin \alpha \cos \alpha,$$

$$\frac{r_y^2}{4} = \langle y_b^2 \rangle = \left( \langle x^2 \rangle - \langle x \rangle^2 \right) \sin^2 \alpha + \left( \langle y^2 \rangle - \langle y \rangle^2 \right) \cos^2 \alpha - 2 \left( \langle xy \rangle - \langle x \rangle \langle y \rangle \right) \sin \alpha \cos \alpha. \tag{2.6}$$

It is convenient to introduce centroid-centered coordinates

$$\tilde{x} \equiv x - \langle x \rangle \; ; \quad \tilde{y} \equiv y - \langle y \rangle. \tag{2.7}$$

Figure 2.1 illustrates the relationships between the coordinate systems employed in this model.
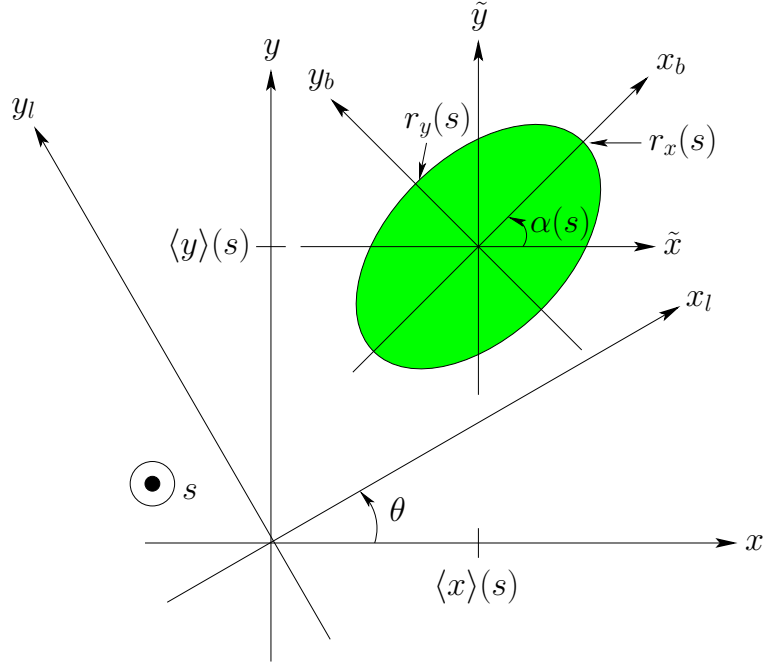
Figure 2.1: Illustration of the relationships between the coordinate systems used

Given any two centroid-centered quantities $\tilde{a}$ and $\tilde{b}$, it is readily shown that

$$\langle \tilde{a}\tilde{b} \rangle = \langle ab \rangle - \langle a \rangle \langle b \rangle. \tag{2.8}$$

Thus, we have

$$\begin{aligned}
\frac{r_x^2}{4} &= \langle x_b^2 \rangle = \langle \tilde{x}^2 \rangle \cos^2 \alpha + \langle \tilde{y}^2 \rangle \sin^2 \alpha + 2\langle \tilde{x}\tilde{y} \rangle \sin \alpha \cos \alpha, \\
\frac{r_y^2}{4} &= \langle y_b^2 \rangle = \langle \tilde{x}^2 \rangle \sin^2 \alpha + \langle \tilde{y}^2 \rangle \cos^2 \alpha - 2\langle \tilde{x}\tilde{y} \rangle \sin \alpha \cos \alpha.
\end{aligned} \tag{2.9}$$

In an actual beam transport lattice suitable for heavy ion fusion, the beams generally occupy the majority of the beam pipe. As such, the beams will in principle be subjected to image charge effects. However, such effects tend to average out over a lattice period, and as a first approximation we will neglect image term contributions in the model developed.

The beam potential in Eq. (2.5) is expressed in terms of $x_b$ and $y_b$. The chain rule

is then applied with Eqs. (2.1) and (2.4) to express the beam particle equations of motion

in the lab frame [19, 20]:

$$x'' = -\frac{(\gamma_b \beta_b)'}{\gamma_b \beta_b} x' - K_{fxx} x - K_{fxy} y + K_{sxx}(x - \langle x \rangle) + K_{sxy}(y - \langle y \rangle),$$

$$y'' = -\frac{(\gamma_b \beta_b)'}{\gamma_b \beta_b} y' - K_{fyy} y - K_{fyx} x + K_{syy}(y - \langle y \rangle) + K_{syx}(x - \langle x \rangle).$$

(2.10)

All the quantities above vary in $s$. The various $K$ functions are defined as follows:

$$K_{fxx} \equiv \kappa_x \cos^2 \theta + \kappa_y \sin^2 \theta,$$

$$K_{fxy} \equiv (\kappa_x - \kappa_y) \sin \theta \cos \theta,$$

$$K_{fyx} \equiv (\kappa_x - \kappa_y) \sin \theta \cos \theta = K_{fxy},$$

$$K_{fyy} \equiv \kappa_y \cos^2 \theta + \kappa_x \sin^2 \theta,$$

$$K_{sxx} \equiv K_{sxb} \cos^2 \alpha + K_{syb} \sin^2 \alpha,$$

(2.11)

$$K_{sxy} \equiv (K_{sxb} - K_{syb}) \sin \alpha \cos \alpha,$$

$$K_{syx} \equiv (K_{sxb} - K_{syb}) \sin \alpha \cos \alpha = K_{sxy},$$

$$K_{syy} \equiv K_{syb} \cos^2 \alpha + K_{sxb} \sin^2 \alpha,$$

where $\kappa_x$ and $\kappa_y$ are the lattice focusing functions discussed earlier,

$$K_{sxb} \equiv \frac{2Q}{(r_x + r_y)r_x},$$

$$K_{syb} \equiv \frac{2Q}{(r_x + r_y)r_y},$$

(2.12)

and

$$Q = \frac{q\lambda}{2\pi\epsilon_0 m \gamma_b^3 \beta_b^2 c^2} = \frac{qI}{2\pi\epsilon_0 m c^3 \gamma_b^3 \beta_b^3}.$$

(2.13)

Here, $I$ denotes the beam current. $Q$ is termed the dimensionless perveance, and provides

a measure of beam space-charge strength [3]. It will, in general, vary in $s$, but if the beam

propagates at a constant velocity and has a constant line charge, $Q$ is constant. Note that

the $K$ functions all have subscripts beginning with $f$ or $s$. An initial $f$ subscript means the function is related to applied focusing terms, while an initial $s$ subscript means the function is related to space-charge terms.

From Eq. (2.10), we see that the first-order moments (i.e. the centroid coordinates and angles in the lab frame) evolve as follows:

$$
\frac{d}{ds}
\begin{pmatrix}
\langle x \rangle \\[6pt]
\langle y \rangle \\[6pt]
\langle x' \rangle \\[6pt]
\langle y' \rangle
\end{pmatrix}
=
\begin{pmatrix}
\langle x' \rangle \\[6pt]
\langle y' \rangle \\[6pt]
-\frac{(\gamma_b \beta_b)'}{\gamma_b \beta_b} \langle x' \rangle - K_{fxx}\langle x \rangle - K_{fxy}\langle y \rangle \\[6pt]
-\frac{(\gamma_b \beta_b)'}{\gamma_b \beta_b} \langle y' \rangle - K_{fyy}\langle y \rangle - K_{fyx}\langle x \rangle
\end{pmatrix}.
\tag{2.14}
$$

For convenience, we express the second-order moments in terms of centroid-frame coordinates $\tilde{x}$ and $\tilde{y}$. Combining the chain rule with Eqs. (2.10) and (2.8) yields the following equations for second-order moment evolution:

$$
\frac{d}{ds}
\begin{pmatrix}
\langle \tilde{x}^2 \rangle \\[6pt]
\langle \tilde{x}\tilde{x}' \rangle \\[6pt]
\langle \tilde{x}'^2 \rangle \\[6pt]
\langle \tilde{y}^2 \rangle \\[6pt]
\langle \tilde{y}\tilde{y}' \rangle \\[6pt]
\langle \tilde{y}'^2 \rangle \\[6pt]
\langle \tilde{x}\tilde{y} \rangle \\[6pt]
\langle \tilde{x}'\tilde{y} \rangle \\[6pt]
\langle \tilde{x}\tilde{y}' \rangle \\[6pt]
\langle \tilde{x}'\tilde{y}' \rangle
\end{pmatrix}
=
\begin{pmatrix}
2\langle \tilde{x}\tilde{x}' \rangle \\[6pt]
\langle \tilde{x}'^2 \rangle + K_{xx}\langle \tilde{x}^2 \rangle + K_{xy}\langle \tilde{x}\tilde{y} \rangle - \frac{(\gamma_b \beta_b)'}{\gamma_b \beta_b}\langle \tilde{x}\tilde{x}' \rangle \\[6pt]
2K_{xx}\langle \tilde{x}\tilde{x}' \rangle + 2K_{xy}\langle \tilde{x}'\tilde{y} \rangle - 2\frac{(\gamma_b \beta_b)'}{\gamma_b \beta_b}\langle \tilde{x}'^2 \rangle \\[6pt]
2\langle \tilde{y}\tilde{y}' \rangle \\[6pt]
\langle \tilde{y}'^2 \rangle + K_{yy}\langle \tilde{y}^2 \rangle + K_{yx}\langle \tilde{x}\tilde{y} \rangle - \frac{(\gamma_b \beta_b)'}{\gamma_b \beta_b}\langle \tilde{y}\tilde{y}' \rangle \\[6pt]
2K_{yy}\langle \tilde{y}\tilde{y}' \rangle + 2K_{yx}\langle \tilde{x}\tilde{y}' \rangle - 2\frac{(\gamma_b \beta_b)'}{\gamma_b \beta_b}\langle \tilde{y}'^2 \rangle \\[6pt]
\langle \tilde{x}'\tilde{y} \rangle + \langle \tilde{x}\tilde{y}' \rangle \\[6pt]
\langle \tilde{x}'\tilde{y}' \rangle + K_{xx}\langle \tilde{x}\tilde{y} \rangle + K_{xy}\langle \tilde{y}^2 \rangle - \frac{(\gamma_b \beta_b)'}{\gamma_b \beta_b}\langle \tilde{x}'\tilde{y} \rangle \\[6pt]
\langle \tilde{x}'\tilde{y}' \rangle + K_{yy}\langle \tilde{x}\tilde{y} \rangle + K_{yx}\langle \tilde{x}^2 \rangle - \frac{(\gamma_b \beta_b)'}{\gamma_b \beta_b}\langle \tilde{x}\tilde{y}' \rangle \\[6pt]
K_{xx}\langle \tilde{x}\tilde{y}' \rangle + K_{xy}\langle \tilde{y}\tilde{y}' \rangle + K_{yy}\langle \tilde{x}'\tilde{y} \rangle + K_{yx}\langle \tilde{x}\tilde{x}' \rangle - 2\frac{(\gamma_b \beta_b)'}{\gamma_b \beta_b}\langle \tilde{x}'\tilde{y}' \rangle
\end{pmatrix},
\tag{2.15}
$$

where

$$K_{xx} \equiv K_{sxx} - K_{fxx},$$

$$K_{yy} \equiv K_{syy} - K_{fyy},$$

$$K_{xy} \equiv K_{sxy} - K_{fxy}, \qquad (2.16)$$

$$K_{yx} \equiv K_{syx} - K_{fyx} = K_{xy}.$$

The rotation angle $\alpha$ of the elliptical beam can be expressed in terms of second-order beam moments, and thus need not be specified explicitly. From Eq. (2.4), we have

$$\langle \tilde{x}^2 \rangle - \langle \tilde{y}^2 \rangle = \left( \langle x_b^2 \rangle - \langle y_b^2 \rangle \right) \cos 2\alpha, \qquad (2.17)$$

and

$$2\langle \tilde{x}\tilde{y} \rangle = \left( \langle x_b^2 \rangle - \langle y_b^2 \rangle \right) \sin 2\alpha, \qquad (2.18)$$

so that

$$\tan 2\alpha = \frac{2\langle \tilde{x}\tilde{y} \rangle}{\langle \tilde{x}^2 \rangle - \langle \tilde{y}^2 \rangle}. \qquad (2.19)$$

The formula above is useful when solving for the various second-order beam moments numerically.

Equations (2.14) and (2.15) represent closed systems of first and second-order beam moments, respectively. The $K_f$ functions depend only on the lattice focusing functions $\kappa_j$ and the lattice misalignment angle $\theta$, all of which are regarded as specified in the lattice description. Similarly, the $K_s$ functions depend on $Q$, $r_j$, and $\alpha$. $Q$ is independent of beam moments, while $r_j$ and $\alpha$ can be expressed in terms of second-order moments. Thus, both Eqs. (2.14) and (2.15) are closed. This closure results from the assumption of a uniform density elliptical beam (possibly rotating and with varying ellipticity) for all values of $s$.

Although such an assumption is not correct for smooth, non-KV distributions, it is expected

to provide a reasonable approximation at high space-charge intensities.

## 2.2  KV equations

For simplicity, assume a system in which both the focusing elements and beam

profile are aligned with the lab frame, i.e. $\theta = \alpha = 0$. This implies that $x_l = x$, $y_l = y$,

$x_b = \tilde{x}$ and $y_b = \tilde{y}$. In this case, the equations of motion in the centroid-centered frame [see

Eqs. (2.10)–(2.12)] reduce to

$$\tilde{x}''(s) + \frac{(\gamma_b \beta_b)'}{\gamma_b \beta_b} \tilde{x}'(s) + \left\{ \kappa_x(s) - \frac{2Q}{[r_x(s) + r_y(s)]\, r_x(s)} \right\} \tilde{x}(s) = 0,$$

$$\tilde{y}''(s) + \frac{(\gamma_b \beta_b)'}{\gamma_b \beta_b} \tilde{y}'(s) + \left\{ \kappa_y(s) - \frac{2Q}{[r_x(s) + r_y(s)]\, r_y(s)} \right\} \tilde{y}(s) = 0. \tag{2.20}$$

In this case, the beam envelope's semi-axes $r_x$ and $r_y$ are related simply to second order

centroid moments by [see Eq. (2.9) with $\alpha = 0$] [3]

$$r_x \equiv 2\sqrt{\langle \tilde{x}^2 \rangle}, \qquad r_y \equiv 2\sqrt{\langle \tilde{y}^2 \rangle}. \tag{2.21}$$

Other useful quantities related to second order beam moments in each plane are

the rms edge emittances [3]

$$\varepsilon_x \equiv 4 \left[ \langle \tilde{x}^2 \rangle \langle \tilde{x}'^2 \rangle - \langle \tilde{x}\tilde{x}' \rangle^2 \right]^{1/2},$$

$$\varepsilon_y \equiv 4 \left[ \langle \tilde{y}^2 \rangle \langle \tilde{y}'^2 \rangle - \langle \tilde{y}\tilde{y}' \rangle^2 \right]^{1/2}. \tag{2.22}$$

The emittances provide a statistical measure of beam phase-space area in the $\tilde{x}$–$\tilde{x}'$ and

$\tilde{y}$–$\tilde{y}'$ planes [21]. The emittances are commonly employed to measure thermal defocusing

forces acting on the beam. In general, the emittances will evolve in $s$ for smooth Vlasov

distributions $f$.

Differentiating Eq. (2.21) once with respect to $s$ obtains

$$\langle \tilde{x}^2 \rangle' = 2\langle \tilde{x}\tilde{x}' \rangle = \frac{r_x r_x'}{2}, \tag{2.23}$$

and twice yields

$$\langle \tilde{x}^2 \rangle'' = 2\langle \tilde{x}'^2 \rangle + 2\langle \tilde{x}\tilde{x}'' \rangle = \frac{r_x'^2}{2} + \frac{r_x r_x''}{2}. \tag{2.24}$$

Combining Eqs. (2.21)–(2.24) reveals that

$$\langle \tilde{x}\tilde{x}'' \rangle = \frac{r_x r_x''}{4} - \frac{\varepsilon_x^2}{4r_x^2}. \tag{2.25}$$

The $\tilde{y}$-plane equations are analogous.

Equations describing the transverse statistical beam envelope evolution may be derived from the equations of motion as follows. The upper of Eq. (2.20) is multiplied by $\tilde{x}$, while the lower is multiplied by $\tilde{y}$. Taking the transverse statistical average of both equations, employing Eqs. (2.23) and (2.25), and factoring out common terms yields the KV envelope equations with acceleration [21]:

$$r_j''(s) + \frac{(\gamma_b \beta_b)'}{\gamma_b \beta_b} r_j'(s) + \kappa_j(s) r_j(s) - \frac{2Q(s)}{r_x(s) + r_y(s)} - \frac{\varepsilon_j^2(s)}{r_j^3(s)} = 0. \tag{2.26}$$

Here, the subscript $j$ denotes either transverse coordinate $x$ or $y$.

If the beam moves at constant velocity (i.e., $\beta_b$ and $\gamma_b$ are constant) the acceleration term vanishes, yielding the more familiar form of the KV envelope equations [3, 21]:

$$r_j''(s) + \kappa_j(s) r_j(s) - \frac{2Q}{r_x(s) + r_y(s)} - \frac{\varepsilon_j^2}{r_j^3(s)} = 0. \tag{2.27}$$

In this limit, $Q$ is constant (assuming that the beam line charge and current are constant as well) as are the emittances $\varepsilon_j$. The fact that constant beam velocity implies constant emittances follows from the definition of emittance [see Eq. (2.22)] and the equations of

motion in the centroid-centered frame without acceleration [see Eq. (2.20)]. These results are consistent with the Vlasov equation only for the KV distribution [22, 23], which is a singular function of Courant-Snyder invariants. This singular structure can lead to unphysical instabilities within the Vlasov model [24]. However, if the $s$-variation of the $\varepsilon_j$ has negligible effect on the $r_j$, then the KV envelope equations can be applied with $\varepsilon_j = $ const to reliably model practical machines. This must generally be verified *a posteriori* with simulations of the full distribution [25].

Provided that the focusing lattices do not exhibit skew coupling, Eq. (2.27) can be employed to model a wide range of transport channels, including solenoidal and quadrupole transport. For solenoidal transport, the equations must be interpreted in a rotating Larmor frame (see Appendix A of Ref. [5]). In a periodic transport lattice, the $\kappa_j$ are periodic with fundamental lattice period $L_p$, i.e.,

$$\kappa_j(s + L_p) = \kappa_j(s). \tag{2.28}$$

If the envelope functions have the same periodicity as the lattice, i.e.,

$$r_j(s + L_p) = r_j(s) \tag{2.29}$$

the beam is defined as matched. For specified focusing functions $\kappa_j(s)$, beam perveance $Q$, and emittances $\varepsilon_j$, the matching condition is equivalent to requiring that $r_j$ and $r'_j$ satisfy specific initial conditions at $s = s_i$ when the envelope equations (2.27) are integrated as an initial value problem. The required initial conditions generally vary with the phase of $s_i$ in the lattice period because the matched solution vaies periodically in $s$. In conventional procedures for envelope matching, needed initial conditions are typically found by numerical

root finding starting from guessed seed values [5]. This numerical matching can be especially problematic when: applied focusing strengths are large, the focusing lattice is complicated and devoid of symmetries that can reduce the dimensionality of the root finding, choices of solution parameters require extra constraints to effect, and where the matched beam envelope is unstable.

If a single particle is only influenced by external, applied fields, its motion in both transverse planes is described by Hill's Equation:

$$x''(s) + \kappa_x(s)x(s) = 0,$$
$$y''(s) + \kappa_y(s)y(s) = 0.$$

(2.30)

Here, $x$ and $y$ denote the transverse particle coordinates. The solution to Hill's Equation can be expressed in matrix form as

$$\begin{pmatrix} x(s) \\ x'(s) \end{pmatrix} = \begin{pmatrix} C_{0x}(s|s_i) & S_{0x}(s|s_i) \\ C'_{0x}(s|s_i) & S'_{0x}(s|s_i) \end{pmatrix} \begin{pmatrix} x(s_i) \\ x'(s_i) \end{pmatrix},$$
$$\begin{pmatrix} y(s) \\ y'(s) \end{pmatrix} = \begin{pmatrix} C_{0y}(s|s_i) & S_{0y}(s|s_i) \\ C'_{0y}(s|s_i) & S'_{0y}(s|s_i) \end{pmatrix} \begin{pmatrix} y(s_i) \\ y'(s_i) \end{pmatrix}.$$

(2.31)

The $2 \times 2$ matrices on the right side of both of the above equations are termed the transfer matrices in the $j$-plane from an initial axial coordinate $s = s_i$ to axial coordinate $s$. These matrices are denoted as

$$\mathbf{M}_{0j}(s|s_i) = \begin{pmatrix} C_{0j}(s|s_i) & S_{0j}(s|s_i) \\ C'_{0j}(s|s_i) & S'_{0j}(s|s_i) \end{pmatrix}.$$

(2.32)

The terms $C_{0j}(s|s_i)$ and $S_{0j}(s|s_i)$ denote cosine-like and sine-like principal orbit functions satisfying

$$F''_{0j}(s|s_i) + \kappa_j(s)F_{0j}(s|s_i) = 0,$$

(2.33)

with $F$ representing $C$ or $S$ with $C_{0j}$ subject to cosine-like initial $(s = s_i)$ conditions $C_{0j}(s_i|s_i) = 1$ and $C'_{0j}(s_i|s_i) = 0$, and with $S_{0j}$ subject to sine-like initial conditions $S_{0j}(s_i|s_i) = 0$ and $S'_{0j}(s_i|s_i) = 1$.

The undepressed particle phase advance per lattice period $\sigma_{0j}$ provides a dimensionless measure of the strength of the applied focusing functions $\kappa_j$ describing the periodic lattice [5, 7]. The $\sigma_{0j}$ can be calculated from [7]

$$\cos \sigma_{0j} = \frac{1}{2}\text{Tr } \mathbf{M}_{0j}(s_i + L_p|s_i) = \frac{1}{2}[C_{0j}(s_i + L_p|s_i) + S'_{0j}(s_i + L_p|s_i)]. \tag{2.34}$$

The $\sigma_{0j}$ are independent of the particular value of $s_i$ used in the calculation of the principal functions. For some particular cases such as piecewise constant $\kappa_j$ the principal functions $F_{0j}$ can be calculated analytically. In general, however, the $F_{0j}$ must be calculated numerically. In the absence of space-charge, the particle orbit is stable whenever $\sigma_{0j} < 180°$ and parametric bands of stability can also be found for $\sigma_{0j} > 180°$ [5, 8]. For a stable orbit, the scale of the $\kappa_j$ (i.e., $\kappa_j \rightarrow \alpha\kappa_j$ with $\alpha = $ const setting the scale of the specified $\kappa_j$) can always be regarded as being set by the $\sigma_{0j}$. In this context, Eq. (2.34) is employed to fix the scale of the $\kappa_j$ in terms of $\sigma_{0j}$ and other parameters defining the $\kappa_j$. Because there appears to be no advantage in using stronger focusing with $\sigma_{0j} > 180°$ in terms of producing more radially compact matched envelopes [5, 26], we will assume in all analysis that follows that the $\kappa_j$ are sufficiently weak to satisfy $\sigma_{0j} < 180°$.

The formulation given above for calculating the undepressed principal orbits $C_{0j}$ and $S_{0j}$ and the undepressed particle phase advances $\sigma_{0j}$ can also be applied to calculate the depressed principal orbits $C_j$ and $S_j$ and the depressed phase advances $\sigma_j$ in the presence of uniform beam space-charge density for a particle moving within the matched KV beam

envelopes. This is done by replacing

$$\kappa_j \to \kappa_j - \frac{2Q}{(r_x + r_y)r_j} \tag{2.35}$$

in Eq. (2.33) and dropping the subscript 0s in Eqs. (2.31)–(2.34) for notational clarity (i.e.,

$C_{0j} \to C_j$ and $S_{0j} \to S_j$). Explicitly, the depressed principal functions satisfy

$$F_j''(s|s_i) + \kappa_j(s)F_j(s|s_i) - \frac{2QF_j(s|s_i)}{[r_x(s) + r_y(s)]r_j(s)} = 0, \tag{2.36}$$

with $F$ representing $C$ or $S$ with $C_j$ subject to $C_j(s_i|s_i) = 1$ and $C_j'(s_i|s_i) = 0$, and $S_j$

subject to $S_j(s_i|s_i) = 0$ and $S_j'(s_i|s_i) = 1$. Analogously to Eq. (2.34), the depressed phase

advances satisfy

$$\cos \sigma_j = \frac{1}{2}[C_j(s_i + L_p|s_i) + S_j'(s_i + L_p|s_i)]. \tag{2.37}$$

For a stable orbit, it can be shown that the $\sigma_j$ can also be calculated from the matched

envelope as [5, 7]

$$\sigma_j = \varepsilon_j \int_{s_i}^{s_i + L_p} \frac{ds}{r_j^2(s)}. \tag{2.38}$$

This formula can also be applied to calculate $\sigma_{0j}$ by using the matched envelope functions

$r_j$ calculated with $Q = 0$.

Phase advances are expressed in units of angle per lattice period. To interpret the

undepressed and depressed phase advances $\sigma_{0j}$ and $\sigma_j$, consider a particle within a matched

beam envelope subject to Hill's Equation either with or without space-charge. Assume

the focusing lattice is stable, i.e. $0° < \sigma_{0j} < 180°$. After some number $n > 2$ of lattice

periods, if the particle returns to its initial conditions, its phase changes by $360°$. The phase

advance of the particle equals $360/n$ degrees per lattice period. Note from Eq. (2.35) that

the space-charge defocusing term in Hill's Equation is a strictly positive function subtracted

from the lattice focusing term, effectively reducing the lattice focusing strength. Thus, the space-charge lengthens the period of a particle orbit within the beam, i.e. it depresses the phase advance. Figure 2.2 illustrates the relationship between depressed and undepressed principal orbits and phase advances for a solenoid focusing lattice with moderate focusing strength and strong space-charge. All plotted quantities are in the Larmor frame.
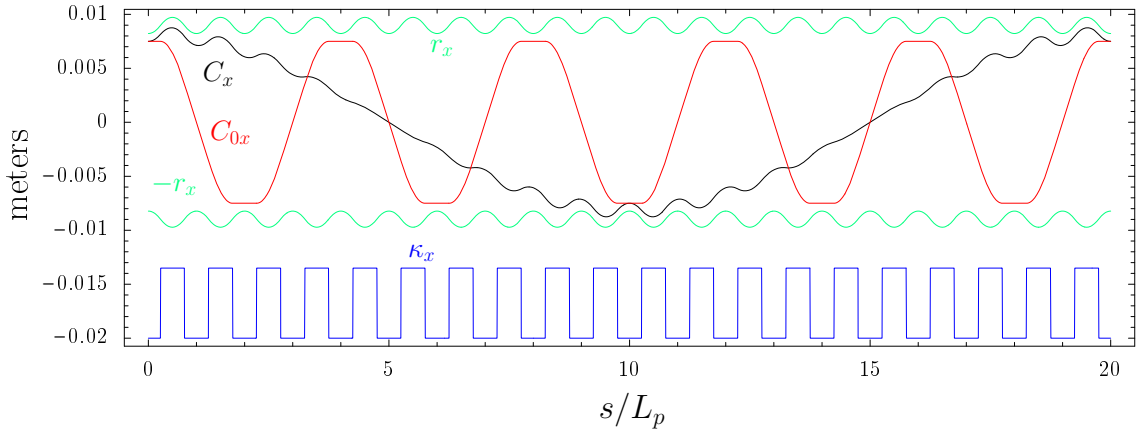


Figure 2.2: Comparison of depressed and undepressed principal orbits for $\sigma_{0x} = 90°$ and $\sigma_x = 18°$. The red and black curves represent rescaled undepressed and depressed x-plane cosine-like principal orbit functions, respectively. The matched beam envelope is plotted in green. The x-plane focusing function is plotted (arbitrary scale) in blue.

To solve the KV equations by any method, the lattice focusing functions $\kappa_j(s)$ and three beam parameters must be specified. Other lattice parameters (period length $L_p$, the fraction $\eta$ of the lattice period occupied by focusing elements, etc.) are specified implicitly through the $\kappa_j$. The undepressed phase advances $\sigma_{0j}$ are regarded as known from the lattice focusing functions $\kappa_j$ and the particle properties ($m$, $q$, $\beta_b$, etc.).

Formally, specifying $Q$, $\varepsilon_x$, and $\varepsilon_y$ is the most natural choice of known beam parameters, since these appear directly in the KV equations (2.27). However, one may also eliminate one or more of the perveance and emittances with the depressed phase advances

$\sigma_j$. Several of these parameterizations are listed in Table 2.1. The expression $\kappa_j$ $(\sigma_{0j})$ indicates that lattice focusing functions may specified explicitly in $s$ or implicitly in $\sigma_{0j}$ if the overall shapes of the $\kappa_j$ are known. It can be convenient, particularly when carrying out parametric surveys (for example, see Ref. [5]) to specify one or more of the $\sigma_j$ because $\sigma_j/\sigma_{0j}$ is a dimensionless measure of space-charge strength satisfying $0 \le \sigma_j/\sigma_{0j} \le 1$ with $\sigma_j/\sigma_{0j} \to 1$ representing a warm beam with negligible space-charge (i.e., $Q \to 0$, or $\varepsilon_j \to \infty$ for finite $Q$), and $\sigma_j/\sigma_{0j} \to 0$ representing a cold beam with maximum space-charge intensity (i.e., $\varepsilon_j \to 0$).

It is assumed that a unique matched envelope solution exists *independent* of the parameterization when the $\kappa_j$ are fully specified. There is no known proof of this conjecture, but numerical evidence suggests that it is correct for simple focusing lattices (i.e., simple $\kappa_j$) when $\sigma_{0j} < 180°$. In typical experimental situations, note that transport lattices are fixed in geometry and excitations of focusing elements in the lattices can be individually adjusted. In the language adopted here, such lattices with different excitations in focusing elements (both overall scale and otherwise) correspond to different lattices described by distinct $\kappa_j$ with corresponding matched envelopes.

Table 2.1: Common possible parameterizations of matched envelope solutions.

| Case | Parameters |
| --- | --- |
| 0 | $\kappa_j\ (\sigma_{0j})$, $Q$, $\varepsilon_x$, $\varepsilon_y$ |
| 1 | $\kappa_j\ (\sigma_{0j})$, $Q$, $\sigma_x$, $\sigma_y$ |
| 2 | $\kappa_j\ (\sigma_{0j})$, $\varepsilon_x = \varepsilon_y$, $\sigma_x = \sigma_y$ |
| 2a | $\kappa_j\ (\sigma_{0j})$, $\varepsilon_x$, $\varepsilon_y$, $\sigma_x$ |
| 2b | $\kappa_j\ (\sigma_{0j})$, $\varepsilon_x$, $\varepsilon_y$, $\sigma_y$ |
| 3a | $\kappa_j\ (\sigma_{0j})$, $\varepsilon_x$, $\sigma_x$, $\sigma_y$ |
| 3b | $\kappa_j\ (\sigma_{0j})$, $\varepsilon_y$, $\sigma_x$, $\sigma_y$ |

# Chapter 3

# Matched Envelope Properties

In developing the IM method in Chapter 4, we employ a consistency condition between depressed particle orbits within the beam and the matched envelope functions (Sec. 3.1) and use a continuous focusing description of the matched beam (Sec. 3.2) as part of the formulation to generate a seed iteration. The IM method does not apply to lattices with skew coupled focusing elements. Acceleration is also neglected because, strictly speaking, it precludes exact periodicity. However, acceleration effects are often negligible in one lattice period [i.e., $(\gamma_b \beta_b)'$ small].

## 3.1 Consistency Condition

The matching method employs a consistency condition between the matched envelope radial function $r_j$ and the depressed principal orbit functions $C_j$ and $S_j$. The consistency condition is derived as follows. First, the transfer matrix $\mathbf{M}_j$ of the depressed particle

orbit in the $j$-plane is expressed in terms of betatron function-like formulation as [7]

$$\mathbf{M}_j(s|s_i) = \begin{pmatrix} C_j(s|s_i) & S_j(s|s_i) \\ \\ C'_j(s|s_i) & S'_j(s|s_i) \end{pmatrix} \tag{3.1}$$

with

$$C_j(s|s_i) = \frac{r_j(s)}{r_j(s_i)} \cos \Delta\psi_j(s) - \frac{r'_j(s_i)r_j(s)}{\varepsilon_j} \sin \Delta\psi_j(s),$$

$$S_j(s|s_i) = \frac{r_j(s_i)r_j(s)}{\varepsilon_j} \sin \Delta\psi_j(s),$$

$$C'_j(s|s_i) = \left[ \frac{r'_j(s)}{r_j(s_i)} - \frac{r'_j(s_i)}{r_j(s)} \right] \cos \Delta\psi_j(s) \tag{3.2}$$

$$- \left[ \frac{\varepsilon_j}{r_j(s_i)r_j(s)} + \frac{r'_j(s_i)r'_j(s)}{\varepsilon_j} \right] \sin \Delta\psi_j(s),$$

$$S'_j(s|s_i) = \frac{r_j(s_i)}{r_j(s)} \cos \Delta\psi_j(s) + \frac{r_j(s_i)r'_j(s)}{\varepsilon_j} \sin \Delta\psi_j(s).$$

Here,

$$\Delta\psi_j(s) = \varepsilon_j \int_{s_i}^{s} \frac{d\tilde{s}}{r_j^2(\tilde{s})} \tag{3.3}$$

is the change in betatron phase of the particle orbit from $s = s_i$ to $s$ and the principal functions $C_j$ and $S_j$ are calculated including the linear space-charge term of the uniform density elliptical beam from Eq. (2.36). Note that $r_j \equiv \sqrt{\varepsilon_j \beta_j}$ can be used in Eqs. (3.2) and (3.3) to express the results in terms of the betatron amplitude functions $\beta_j$ describing linear orbits internal to the beam in the $j$-plane [7]. These generalized betatron functions are periodic [i.e., $\beta_j(s + L_p) = \beta_j(s)$] and include the transverse defocusing effects of uniformly distributed space-charge within the KV equilibrium envelope.

Isolating $\cos \Delta\psi_j(s)$ and $\sin \Delta\psi_j(s)$ in Eq. (3.2), invoking the Pythagorean Identity, and collecting terms yields

$$\beta_j(s) = \frac{r_j^2(s)}{\varepsilon_j} = \frac{\varepsilon_j}{r_j^2(s_i)} S_j^2(s|s_i) + \frac{r_j^2(s_i)}{\varepsilon_j} \left[ C_j(s|s_i) + \frac{r'_j(s_i)}{r_j(s_i)} S_j(s|s_i) \right]^2. \tag{3.4}$$

The periodicity of $r_j(s)$ and $r_j'(s)$ and the fact that $\Delta\psi_j(s_i + L_p) = \sigma_j$ allows us to express $r_j(s_i)$ and $r_j'(s_i)$ as

$$r_j(s_i) = \sqrt{\frac{\varepsilon_j S_j(s_i + L_p|s_i)}{\sin\sigma_j}} \qquad (3.5)$$

and

$$r_j'(s_i) = \sqrt{\frac{\varepsilon_j}{\sin\sigma_j S_j(s_i + L_p|s_i)}} \left[ \cos\sigma_j - C_j(s_i + L_p|s_i) \right]. \qquad (3.6)$$

Substituting Eqs. (3.5) and (3.6) into Eq. (3.4) obtains the following consistency condition between the matched envelope radii and principal orbits:

$$
\begin{aligned}
\beta_j(s) = \frac{r_j^2(s)}{\varepsilon_j} =& \frac{S_j^2(s|s_i)}{S_j(s_i + L_p|s_i)/\sin\sigma_j} \\
&+ \frac{S_j(s_i + L_p|s_i)}{\sin\sigma_j} \left[ C_j(s|s_i) + \frac{\cos\sigma_j - C_j(s_i + L_p|s_i)}{S_j(s_i + L_p|s_i)} S_j(s|s_i) \right]^2.
\end{aligned}
\qquad (3.7)
$$

Equation (3.7) shows that the linear principal functions $C_j$ and $S_j$ need only be calculated in $s$ from some arbitrary initial point $(s_i)$ over *one* lattice period (to $s_i + L_p$) to specify the consistency condition for the matched envelope functions $r_j(s)$, or equivalently, the betatron amplitude functions $\beta_j(s) = r_j^2(s)/\varepsilon_j$. Equation (3.7) can also be derived using Courant-Snyder invariants of particle orbits within the beam.

As the equations above show, the matched radial functions $r_j$ can be calculated from the principal orbits $F_j$. However, the ODE governing principal orbit evolution depends on the matched radii. Solving a coupled system of KV and principal orbit equations is more difficult than the original problem of finding matched solutions to the KV equations. However, this system can be solved via an iterative approach, as illustrated in Chapter 4, to obtain a superior numerical matching method.

## 3.2 Continuous Limit

In the continuous limit, we treat the lattice focusing functions as constants, i.e. we make the substitution

$$\kappa_j \rightarrow \left(\frac{\sigma_{0j}}{L_p}\right)^2. \tag{3.8}$$

Here, the $\sigma_{0j}$ are the undepressed phase advances of the actual $s$-varying lattice focusing functions. Denote the lattice period average as

$$\overline{\zeta} \equiv \int_{s_i}^{s_i+L_p} \frac{ds}{L_p}\zeta(s). \tag{3.9}$$

The matched envelope satisfies $\overline{r_j} = \text{const}$ (as does the period average of and function of $s$ alone), and since the matched $r_j$ have the same periodicity as the lattice, $\overline{r_j''} = 0$.

In the continuous limit, we replace $r_j \rightarrow \overline{r_j}$, $r_j'' \rightarrow 0$ and Eq. (3.8) into the KV equations (2.27) to obtain

$$\left(\frac{\sigma_{0j}}{L_p}\right)^2 \overline{r_j} - \frac{2Q}{\overline{r_x}+\overline{r_y}} - \frac{\varepsilon_j^2}{\overline{r_j}^3} = 0. \tag{3.10}$$

In applications, the continuous limit solution described by Eqs. (3.8)–(3.10) must be solved under the various parameterizations in Sec. 2.2 (see Table 2.1). For example, if the emittances and depressed phase advances are known, and we replace $r_j$ with $\overline{r_j}$ in Eq. (2.38), then

$$\overline{r_j} = \sqrt{\frac{\varepsilon_j}{(\sigma_j/L_p)}}. \tag{3.11}$$

If $Q$ and $\varepsilon_j$ are known, the continuous limit radii may be solved directly from Eq. (3.10). If the the system is plane-symmetric, i.e. $\sigma_{0x} = \sigma_{0y} = \sigma_0$ and $\varepsilon_x = \varepsilon_y = \varepsilon$, then $\overline{r_x} = \overline{r_y} \equiv \overline{r_b}$. In this case, the continuous limit envelope equations decouple, yielding

a quadratic equation in $\overline{r_b}^2$. This equation is easily solved as

$$\overline{r_b} = \frac{1}{(\sigma_0/L_p)} \left[ \frac{Q}{2} + \frac{1}{2}\sqrt{Q^2 + 4\left(\frac{\sigma_0}{L_p}\right)^2 \varepsilon^2} \right]^{1/2}. \tag{3.12}$$

If the lattice focusing system is not plane-symmetric, $\overline{r_x}$ and $\overline{r_y}$ can be solved numerically via Newton root finding, with $\overline{r_b}$ as calculated above as the starting guess.

If the emittances $\varepsilon_j$ are unknown, but the phase advances and perveance are known, we rewrite Eq. (3.11) as

$$\left(\frac{\sigma_j}{L_p}\right)^2 \overline{r_j} - \frac{\varepsilon_j^2}{\overline{r_j}^3} = 0 \tag{3.13}$$

and combine the formula above with Eq. (3.10) to eliminate the emittance terms, yielding

$$\begin{aligned}
\left(\frac{\sigma_x}{L_p}\right)^2 \overline{r_x} &= \left(\frac{\sigma_{0x}}{L_p}\right)^2 \overline{r_x} - \frac{2Q}{\overline{r_x} + \overline{r_y}}, \\
\left(\frac{\sigma_y}{L_p}\right)^2 \overline{r_y} &= \left(\frac{\sigma_{0y}}{L_p}\right)^2 \overline{r_y} - \frac{2Q}{\overline{r_x} + \overline{r_y}}.
\end{aligned} \tag{3.14}$$

Straightforward algebra shows that

$$\frac{\overline{r_y}}{\overline{r_x}} = \frac{\sigma_{0x}^2 - \sigma_x^2}{\sigma_{0y}^2 - \sigma_y^2}. \tag{3.15}$$

Substituting this ratio back into Eq. (3.14) yields

$$\begin{aligned}
\overline{r_x} &= \frac{\sqrt{2Q}L_p}{\sqrt{(\sigma_{0x}^2 - \sigma_x^2) + \frac{(\sigma_{0x}^2 - \sigma_x^2)^2}{(\sigma_{0y}^2 - \sigma_y^2)}}}, \\
\overline{r_y} &= \frac{\sqrt{2Q}L_p}{\sqrt{(\sigma_{0y}^2 - \sigma_y^2) + \frac{(\sigma_{0y}^2 - \sigma_y^2)^2}{(\sigma_{0x}^2 - \sigma_x^2)}}}.
\end{aligned} \tag{3.16}$$

The continuous limit emittances $\overline{\varepsilon_j}$ can then be defined in terms of the $\overline{r_j}$ by inverting Eq. (3.11) and taking $\varepsilon_j \to \overline{\varepsilon_j}$.

If the perveance $Q$ is unknown, it can be useful to define a continuous limit value $\overline{Q}$ by replacing $Q \to \overline{Q}$ in Eq. (3.14) to obtain

$$
\begin{aligned}
\overline{Q} &= \frac{\left(\sigma_{0x}^2 - \sigma_x^2\right)\left(\overline{r_x} + \overline{r_y}\right)\overline{r_x}}{2L_p^2} \\
&= \frac{\left(\sigma_{0y}^2 - \sigma_y^2\right)\left(\overline{r_x} + \overline{r_y}\right)\overline{r_y}}{2L_p^2}.
\end{aligned}
\tag{3.17}
$$

Typically, we express $\overline{Q}$ as the average of the two equations above to improve accuracy in numerical calculations.

It is sometimes convenient to combine Eq. (3.10) to eliminate the space-charge defocusing terms proportional to $Q$ to obtain

$$
\left(\frac{\sigma_{0y}}{L_p}\right)^2 \overline{r_y} - \left(\frac{\sigma_{0x}}{L_p}\right)^2 \overline{r_x} - \frac{\varepsilon_y^2}{\overline{r_y}^3} + \frac{\varepsilon_x^2}{\overline{r_x}^3} = 0.
\tag{3.18}
$$

In some cases, the continuous limit radii must be calculated by different methods. For example, one of the $\overline{r_j}$ may be given by Eq. (3.11), while the other is then solved from Eq. (3.18) via Newton root finding, using the known value of $\overline{r_j}$ as a starting guess. In other cases, the second $\overline{r_j}$ is solved from Eq. (3.15) instead. However, Eqs. (3.10)–(3.18) are sufficient for finding any unknown continuous limit parameters and radii, regardless of which parameters are known at the outset.

# Chapter 4

# Iterative Matching Method

An iterative matching method is formulated based on calculating principal orbits in an initial (seed iteration) assumed envelope and then using the consistency condition (3.7) to update the envelope radii. The process is seeded, using an envelope with space-charge based on the continuous limit combined with the actual (applied) periodic focusing lattice, and then iterated until a fractional error tolerance is met. The process is structured as illustrated in Fig. 4.1
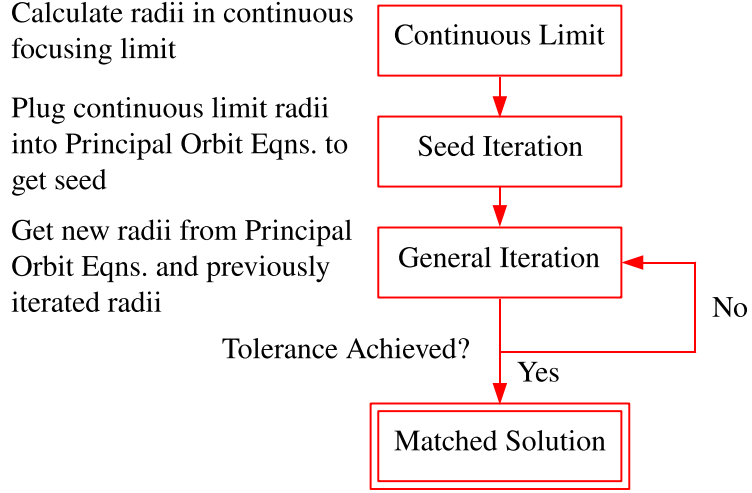
Figure 4.1: Schematic of matching method

We formulate the method as follows. Denote the iteration order by a superscript $i = 0, 1, 2, \ldots$ The betatron consistency condition (3.7) for the $i$th iteration is expressed as

$$
\begin{aligned}
\beta_j^i(s) = \frac{[r_j^i(s)]^2}{\varepsilon_j^i} =& \frac{[S_j^i(s|s_i)]^2}{S_j^i(s_i + L_p|s_i)/\sin \sigma_j^i} \\
&+ \frac{S_j^i(s_i + L_p|s_i)}{\sin \sigma_j^i} \left[ C_j^i(s|s_i) + \frac{\cos \sigma_j^i - C_j^i(s_i + L_p|s_i)}{S_j^i(s_i + L_p|s_i)} S_j^i(s|s_i) \right]^2 .
\end{aligned}
\tag{4.1}
$$

Here, all quantities associated with the iteration are superscripted. If the emittances and/or the depressed phase advances are specified, $\varepsilon_j^i \equiv \varepsilon_j$ and/or $\sigma_j^i \equiv \sigma_j$ for all iteration orders.

The principal orbits of the $i$th iteration for $i \geq 1$ are calculated from the previous iteration by solving

$$
F_j^{i\,\prime\prime} + \left[ \kappa_j - \frac{2Q^{i-1}}{(r_x^{i-1} + r_y^{i-1})r_j^{i-1}} \right] F_j^i = 0.
\tag{4.2}
$$

Here, $F_j^i$ denotes $C_j^i(s|s_i)$ or $S_j^i(s|s_i)$ subject to the initial ($s = s_i$) conditions $C_j^i(s_i|s_i) = 1$, $C_j^{i\,\prime}(s_i|s_i) = 0$ and $S_j^i(s_i|s_i) = 0$, $S_j^{i\,\prime}(s_i|s_i) = 1$, and $Q^{i-1}$ and $r_j^{i-1}$ denote the perveance and envelope radii calculated in the previous iteration cycle. If $Q$ is specified, then $Q^i \equiv Q$

in all iteration orders.

The seed $(i = 0)$ iteration is formulated as follows. First, the continuous limit envelope radii $\overline{r_j}$ are calculated using the formulation in Sec. 3.2. The seed principle orbits are then calculated from the continuous beam envelope radii $\overline{r_j}$ by solving

$$F_j^{0\,\prime\prime} + \left[\kappa_j - \frac{2\overline{Q}}{(\overline{r_x} + \overline{r_y})\overline{r_j}}\right] F_j^0 = 0. \tag{4.3}$$

Here, $F_j^0$ denotes $C_j^0(s|s_i)$ or $S_j^0(s|s_i)$ subject to the initial $(s = s_i)$ conditions $C_j^0(s_i|s_i) = 1$, $C_j^{0\,\prime}(s_i|s_i) = 0$ and $S_j^0(s_i|s_i) = 0$, $S_j^{0\,\prime}(s_i|s_i) = 1$, and $\overline{Q}$ and $\overline{r_j}$ denote the continuous values of perveance and envelope radii calculated earlier with $Q \to \overline{Q}$ and $\varepsilon_j \to \overline{\varepsilon_j}$. Recall from Sec. 3.2 that $\overline{Q}$ and $\overline{\varepsilon_j}$ may be calculated in several different ways depending on the beam parameters specified. Note also that the seed principal orbits $F_j^0$ are calculated with the actual lattice focusing functions $\kappa_j$ and continuous limit approximate space-charge. The orbits will consequently exhibit the flutter of the matched envelope driven primarily by the variation in applied focusing forces with the average effect of space-charge acting to increase the beam size.

Matched envelope angles for the iteration can be obtained either by numerically differentiating the discretized solutions of the matched radii $r_j^i$ or from the betatron consistency condition. Differentiating the relationship between betatron functions and matched radii, we see that

$$r_j^{i\prime}(s) = \sqrt{\frac{\varepsilon_j^i}{\beta_j^i(s)} \frac{\beta_j^{i\prime}(s)}{2}}. \tag{4.4}$$

Iterations are terminated at some value of $i$ where the maximum fractional change

between $i$ and $(i-1)$ iterations is less than a specified tolerance tol, i.e.

$$\text{Max} \left| \frac{r_j^i - r_j^{i-1}}{r_j^i} \right| \leq \text{tol}, \tag{4.5}$$

where Max denotes the maximum taken over the lattice period $L_p$ and the component index

$j = x, y$.

Unspecified beam parameters must be calculated from those known, either to

solve for $r_j^i$ directly or to compute the principal orbit functions in the subsequent iteration.

For example, when the depressed phase advances $\sigma_j$ are known, we exploit the fact that

$r_j^i(s) = \sqrt{\varepsilon_j^i \beta_j^i(s)}$ to express Eq. (3.10) as follows:

$$\overline{\kappa_x \sqrt{\beta_x^i}} - \frac{2Q^i}{\sqrt{\varepsilon_x^i}} \overline{\frac{1}{\sqrt{\varepsilon_x^i \beta_x^i} + \sqrt{\varepsilon_y^i \beta_y^i}}} - \overline{\frac{1}{(\beta_x^i)^{3/2}}} = 0$$

$$\overline{\kappa_y \sqrt{\beta_y^i}} - \frac{2Q^i}{\sqrt{\varepsilon_y^i}} \overline{\frac{1}{\sqrt{\varepsilon_x^i \beta_x^i} + \sqrt{\varepsilon_y^i \beta_y^i}}} - \overline{\frac{1}{(\beta_y^i)^{3/2}}} = 0. \tag{4.6}$$

Solving for $\overline{\frac{1}{\sqrt{\varepsilon_x^i \beta_x^i} + \sqrt{\varepsilon_y^i \beta_y^i}}}$ in both x- and y-plane versions of Eq. (4.6) and setting both

versions equal yields the following ratio of emittances:

$$\sqrt{\frac{\varepsilon_y^i}{\varepsilon_x^i}} = \frac{\overline{\kappa_x \sqrt{\beta_x^i}} - \overline{(\beta_x^i)^{-3/2}}}{\overline{\kappa_y \sqrt{\beta_y^i}} - \overline{(\beta_y^i)^{-3/2}}}. \tag{4.7}$$

If the perveance $Q$ is unknown, an iterated value $Q^i$ in terms of other beam

quantities is obtained by substituting Eq. (4.7) back into Eq. (4.6). This gives the following

formulas for $Q^i$, i.e. the perveance at a given order of iteration:

$$Q^i = \frac{\varepsilon_x^i}{2} \left( \overline{\kappa_x \sqrt{\beta_x^i}} - \overline{(\beta_x^i)^{-3/2}} \right) \left( \overline{\frac{1}{\sqrt{\beta_x^i} + \sqrt{\frac{\varepsilon_y^i}{\varepsilon_x^i}} \sqrt{\beta_y^i}}} \right)^{-1}$$

$$= \frac{\varepsilon_y^i}{2} \left( \overline{\kappa_y \sqrt{\beta_y^i}} - \overline{(\beta_y^i)^{-3/2}} \right) \left( \overline{\frac{1}{\sqrt{\beta_y^i} + \sqrt{\frac{\varepsilon_x^i}{\varepsilon_y^i}} \sqrt{\beta_x^i}}} \right)^{-1}. \tag{4.8}$$

Equivalently, one can express $Q^i$ as the average of the two equations above. This is typically done in the program to improve accuracy in numerical calculations.

If the emittances $\varepsilon_j$ are not specified, their iteration values $\varepsilon_j^i$ can be calculated as follows using Eq. (4.8):

$$\varepsilon_x^i = \frac{2Q^i}{\kappa_x \sqrt{\beta_x^i} - \left(\beta_x^i\right)^{-3/2}} \frac{1}{\sqrt{\beta_x^i} + \sqrt{\frac{\varepsilon_y^i}{\varepsilon_x^i}}\sqrt{\beta_y^i}} \, ,$$
$$\varepsilon_y^i = \frac{2Q^i}{\kappa_y \sqrt{\beta_y^i} - \left(\beta_y^i\right)^{-3/2}} \frac{1}{\sqrt{\beta_y^i} + \sqrt{\beta_x^i}/\sqrt{\frac{\varepsilon_y^i}{\varepsilon_x^i}}} \, . \tag{4.9}$$

For parameterizations in which both of the $\sigma_j$ are known, the general iterative procedure is straightforward. The iterated radii $r_j^i$ are given at each order by $r_j^i = \sqrt{\varepsilon_j^i \beta_j^i}$. The iterated betatron functions are obtained from Eq. (4.1). Other quantities are iterated as necessary using Eqs. (4.6) – (4.9).

If the one or more of the depressed phase advances $\sigma_j$ are not known, taking

$$\cos \sigma_j^i = \frac{1}{2}[C_j^i(s_i + L_p|s_i) + S_j^{i\prime}(s_i + L_p|s_i)] \tag{4.10}$$

represents a simple approach to generating iterated approximations. However, this approach causes the matching method as illustrated earlier in this section to fail if space-charge is strong. Numerical evidence suggests that if $\sigma_j/\sigma_{0j} \leq 0.5$ , the beam space-charge is great enough for the method to break down. Strong space-charge can result in compressive over-corrections producing iterated principal orbits that are easily depressed to zero phase advance (i.e., $\sigma_j^i = 0$). In this situation, $\sigma_j^i$ becomes complex and we find that Eq. (3.7) can fail to generate an iteration closer to the desired matched envelope solution. For a better understanding of where and why this problem occurs, see Ref. [6].

The iterative matching method is extended to the entire parameter space for parameterizations with one or more of the $\sigma_j$ unknown by treating one of the known parameters (one or two of: $Q$, $\varepsilon_x$, or $\varepsilon_y$) as functions of the unspecified $\sigma_j$ and employing a root-rinding algorithm to determine the $\sigma_j$ needed to yield a value of $Q$ or $\varepsilon_j$ consistent with that specified. These so-called Hybrid Cases are labeled similarly to the parameterizations described in Table 2.1. For example, given a Case 0 parameterization ($Q$, $\varepsilon_x$, $\varepsilon_y$ known), a Hybrid Case 1 parameterization would correspond to holding $Q$ fixed and using the root finding algorithm to determine both $\sigma_j$ such that $\varepsilon_j(\sigma_j) = \varepsilon_j|_{\text{specified}}$ to within a specified fractional numerical tolerance. Similarly, Hybrid Case 2 would correspond to holding the $\varepsilon_j$ fixed and finding $\sigma_j$ such that $Q(\sigma_j) = Q|_{\text{specified}}$ to within a specified fractional numerical tolerance.

# Chapter 5

# Implementation and Verification of Matching Package

## 5.1 Lattice Setup

Before the matching program is run, the user must first set up the lattice focusing functions within WARP by setting lattice description variables within the Python interface. The user must also define beam parameters (charge species, beam current, etc.). This is usually done with an external lattice setup script written in Python. To load a lattice setup script contained in (ascii-compatible) file `lattice_setup.py`, enter

```
% python -i lattice_setup.py
```

in a terminal command line (the `-i` flag keeps Python open after the script is run), or, after opening Python, enter within the Python interface

```
>>> execfile('lattice_setup.py')
```

## 5.2 Matching Package

Most of the matching package is written in Python, as are most WARP routines that do not entail significant amounts of numerical work. All $s$-varying quantities (e.g. envelope radii and angles) are represented as discretized arrays. Several SciPy packages (see Ref. [27]) were imported to augment the standard WARP routines in implementing the matching program. SciPy routines employed include:

- **scipy.integrate** to integrate discretized data using Simpson's Rule. Use: computing period-averaged quantities.

- **scipy.interpolate** to generate interpolating functions from discretized data. Use: interpolating final envelope radii and angles from arrays broken up into subdomains to desired coordinates.

- **scipy.optimize** for root finding. Uses: calculating $\overline{r_j}$ in some parameterizations and determining $\sigma_j$ consistent with specified parameters in hybridized parameterizations.

Modifications were made to WARP's Fortran-based envelope solver, **env.F**. First, functions were added that return the value of either the $x-$ or $y-$plane lattice focusing functions $\kappa_j$ at a single point in the lattice. Subroutines padded on the lattice functions return $\kappa_j$ at an array of points to more efficiently structure Python calls using vector syntax. These functions and subroutines effectively link the matching package to the focusing lattice specified by element descriptions set to define the focusing functions within WARP. Second, a principal orbit equation solver based on the four-stage, fourth-order Runge-Kutta method (RK4) was added [28]. This step was taken because SciPy's ODE solver was too slow.

The Python-based matching package is named `envmatch_KVinvariant.py`. It can be loaded from inside a Python interpreter or script via commands such as

```
>>> import envmatch_KVinvariant
```

or

```
>>> from envmatch_KVinvariant import *
```

The code is well-commented and documented. For information on a function defined within the scope of `envmatch_KVinvariant.py`, the user may either examine the source code or, in a Python interpreter, enter the native Python command

```
>>> help('function_name')
```

or the WARP command

```
>>> doc('function_name')
```

To be clear, `envmatch_KVinvariant.py` consists entirely of function definitions, comments, documentation, and package imports, so the user cannot compute matched solutions to the KV equations merely by loading the package into Python.

A single overarching function called `Match()` computes the matched radii and angles, along with any beam parameters not specified. This function is composed of many nested functions. The matched radii and angles are calculated by calling `Match()` in a Python interpreter or script, via a command of the form

```
>>> outputs = Match(keyword options)
```

The command above is significantly abbreviated. The full tuple of output variables contains over two dozen items. All of the arguments of `Match()` are keyword specified options with reasonable default values, so the function can be called without any arguments in typical

applications. To run the matching program with a non-default input variable value, enter `variable_name = value` between the parentheses in `Match()`. The optional arguments of `Match()` can be set to tune the numerical tolerances or cases of solution parameterization. The keyword option names, descriptions, and default values are listed below:

- `emitx`: real [m-rad]

  Default: 'auto' sets `emitx = top.emitx` from WARP inputs.

  x-plane beam rms edge emittance.

- `emity`: (y-plane analogue of `emitx`)

- `sigmax`: real [rad/period]

  Default: 'auto' sets as appropriate from parameter specification

  x-plane depressed phase advance.

- `sigmay`: (y-plane analogue of `sigmax`)

- `SolCase`: string

  Default: '0' (standard case; corresponds to the usual choice of simulation description in WARP)

  Specifies the solution parameterization. Acceptable values are those given in Table 2.1.

- `HybridCase`: string

  Default: '1'

  Can set to '1' or '2'. Specifies the hybrid parameterization. See the last two paragraphs of Chapter 4.

- `tol`: real [1]

  Default: `1.e-6`

  Maximum fractional difference between successive iterated radial functions in either x- or y-plane to terminate iterations.

- `rftol`: real [1]

  Default: `10*tol`

  Maximum fractional tolerance between two succesive root finding iterations. Used in hybridized root finding. See the last two paragraphs of Chapter 4.

- `LatGen`: logical

  Default: `True`

  If `True`, the matching program extracts all lattice properties needed for the match. Should only set to `False` if the same lattice is used in consecutive simulations. This option exists only for reasons of numerical efficiency if many solutions are calculated. It is ignorable in standard uses.

- `error_stop`: logical

  Default: `True`

  If `True`, the matching program stops if any error trap is tripped and prints a message explaining the problem. If set to `False`, the program keeps running through the error, with possibly unreliable results.

Figures 5.1 and 5.2 show matched solutions to the KV equations calculated by `Match()`. In Fig. 5.1, the beam is focused by a simple FODO quadrupole doublet lattice

with piecewise constant focusing functions $\kappa_j$, lattice period length $L_p = 0.5$ m, and 50%
quadrupole occupancy. In Fig. 5.2, the lattice is again piecewise constant quadrupole fo-
cusing, but considerably more complicated, as illustrated in the figure. Beam parameters
for both lattices are given in Table 5.1. In this table, Lattice 1 refers to the FODO lattice,
while Lattice 2 refers to the more complicated quadrupole lattice. For both lattices, the
period starts at $s_i = 0$.

Table 5.2 lists the total number of IM iterations required to achieve a fractional
tolerance between successively iterated radial functions of $10^{-6}$ for each parameterization
in Table 2.1 for Lattices 1 and 2. In parameterizations that require hybridized root-finding,
all iterations are counted.

Table 5.1: Numerical parameters for matched beams

| Parameters | Lattice 1 | Lattice 2 |
|:---:|:---|:---|
| $Q$ | $5 \times 10^{-4}$ | $5 \times 10^{-4}$ |
| $\varepsilon_x$ | 50 mm-mrad | 50 mm-mrad |
| $\varepsilon_y$ | 50 mm-mrad | 50 mm-mrad |
| $\sigma_{0x}$ | $60°$ | $70.2307°$ |
| $\sigma_{0y}$ | $60°$ | $67.4392°$ |
| $\sigma_x$ | $11.9849°$ | $16.6113°$ |
| $\sigma_y$ | $11.9849°$ | $14.5614°$ |
| $r_x(s = s_i)$ | 11.2712 mm | 11.9947 mm |
| $r_y(s = s_i)$ | 11.2712 mm | 8.1965 mm |
| $r_x'(s = s_i)$ | 28.1276 mrad | 14.9040 mrad |
| $r_y'(s = s_i)$ | -28.1276 mrad | -12.6578 mrad |

Table 5.2: Total iterations required to achieve a tolerance of $10^{-6}$, with 1000 steps per period.

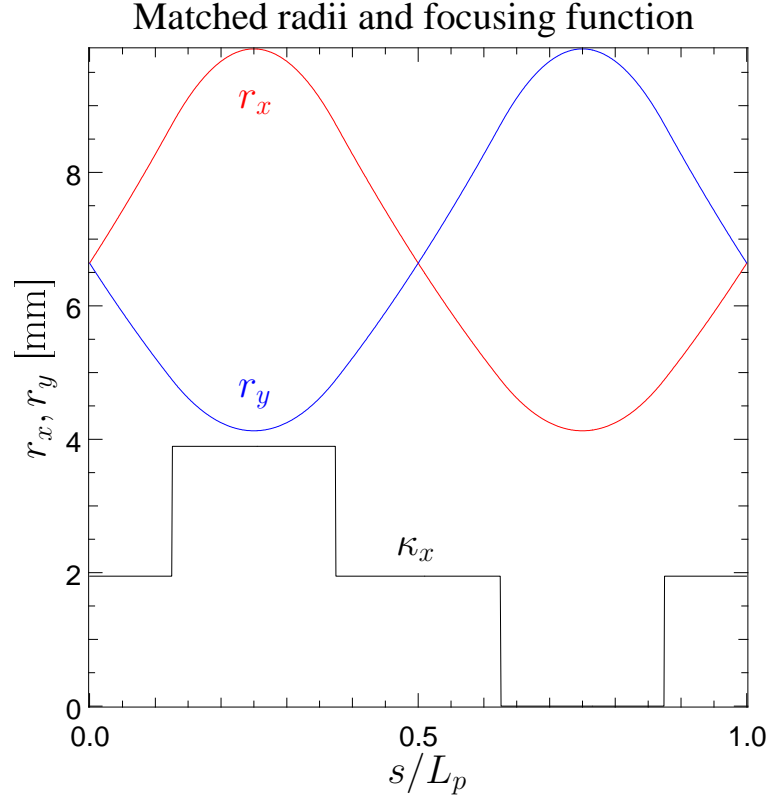| Parameterization | Hybridized | Lattice 1 | Lattice 2 |
|:---:|:---:|:---:|:---:|
| 0 | Yes | 14 | 29 |
| 1 | No | 5 | 9 |
| 2 | No | 5 | 5 |
| 2a | Yes | 16 | 32 |
| 2b | Yes | 16 | 40 |
| 3a | No | 5 | 9 |
| 3b | No | 5 | 9 |

Matched radii and focusing function



Figure 5.1: Matched radial solutions to the KV equations for a FODO quadrupole doublet focusing lattice. A rescaled and shifted $\kappa_x = -\kappa_y$ is plotted as well for comparison. Lattice and beam parameters are given in Table 5.1
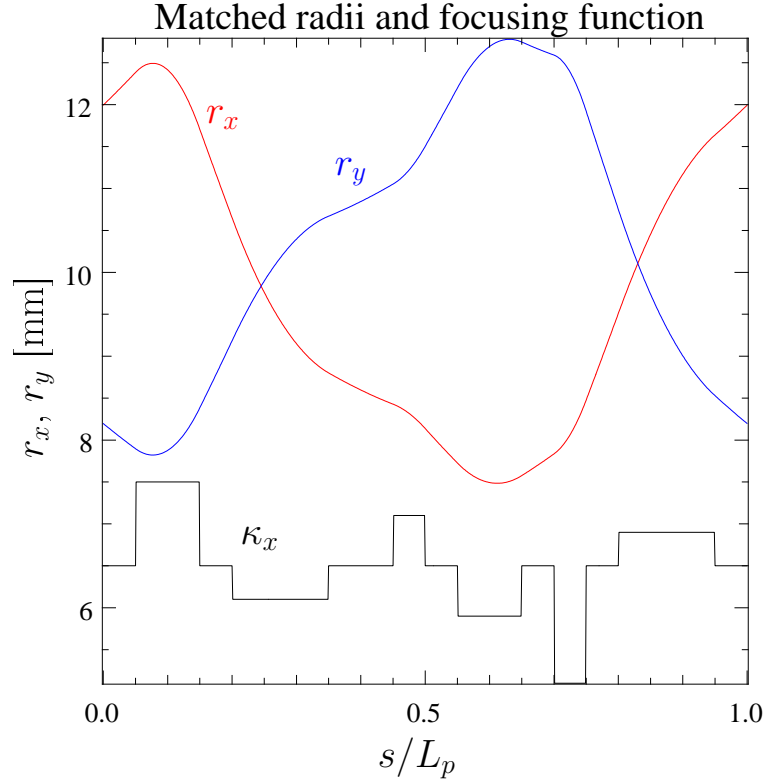
Figure 5.2: Matched radial solutions to the KV equations for a complicated quadrupole focusing lattice. Lattice and beam parameters are given in Table 5.1

## 5.3 Comparison Between Matching Package and Particle-In-Cell Simulations

To assess the validity of the IM method for computing matched solutions to the KV envelope equations, particle beams in initial KV and waterbag distributions (see Ref. [5, 21]) were advanced through WARP's transverse slice PIC code. The KV distribution, a singular function of Courant-Snyder invariants, is the only known Vlasov equilibrium particle distribution fully consistent with the KV equations. The waterbag distribution, on the other hand, is a smooth function of Courant-Snyder invariants and not an exact

Vlasov equilibrium. PIC methods simulate the evolution of Vlasov distribution functions numerically using discretized elements to represent the smooth Vlasov flow. Demonstrating good agreement between macro-particle envelope radii statistically calculated in a PIC simulation with an initial envelope-matched KV distribution and matched envelope radii calculated from the same initial conditions from the KV equations with the IM method thus shows a measure of consistency. However, numerical parameters of the simulation must be chosen for convergence in resolution and statistics for precise agreement.

Figures 5.3 and 5.4 each consist of two plots, depicting fractional differences between envelope radii calculated using the IM method and PIC simulations. In all cases, the beams advanced through the PIC code have initial moments corresponding to the rms-equivalent radii calculated from the KV equations. The PIC envelope deviations plotted in the left half and right of each figure are for initial KV and waterbag distributions, respectively. Numerical parameters for all PIC simulations are given in Table 5.3.

Several factors account for the differences between the envelopes from the KV envelope equations and the PIC simulations illustrated in Figs. 5.3 and 5.4. For example, the KV equations neglect image charge effects, which are included in the PIC simulations. However, the radius of the simulated conducting pipe was set to 100 mm, roughly 10 times that of the envelope radii, to minimize the influence of image charges PIC envelopes. Since the KV distribution is an exact Vlasov equilibrium and fully consistent with the KV envelope equations, one expects arbitrarily good agreement between the KV-matched and simulated envelope radii. However, achieving such converged agreement requires extremely fine numerical parameters in the PIC advance due to the sharp spatial boundaries of the

KV distribution and the need for simultaneous high statistics to limit simulation noise. The more simulation particles and the finer the gridding, the greater the agreement between the KV-matched and PIC envelopes.

Another source of differences between the matched envelopes of the IM method and the PIC simulations lies in the numerical methods employed to advance the ODEs in the IM method and to advance macro-particles in the PIC simulations. The principal orbits in the IM method are calculated numerically by the RK4 method, while the macro-particles in the PIC runs are advanced by a second-order synchronized leapfrog scheme.

The fact that the initial waterbag distribution is not a Vlasov equilibrium and is not fully consistent with the KV envelope equations results in some disagreement between KV-matched envelope radii and the simulated envelope radii. However, the initial beam distribution appears to have a much weaker effect on the fractional deviations between KV-matched and PIC-simulated envelopes than the gridding and statistics. As such, the deviations are not much greater for an initial waterbag distribution than for an initial KV distribution. The relatively weak dependence on the initial beam distribution helps explain why the KV equations are so useful in modeling transverse beam evolution.

Table 5.3: Numerical parameters for PIC runs

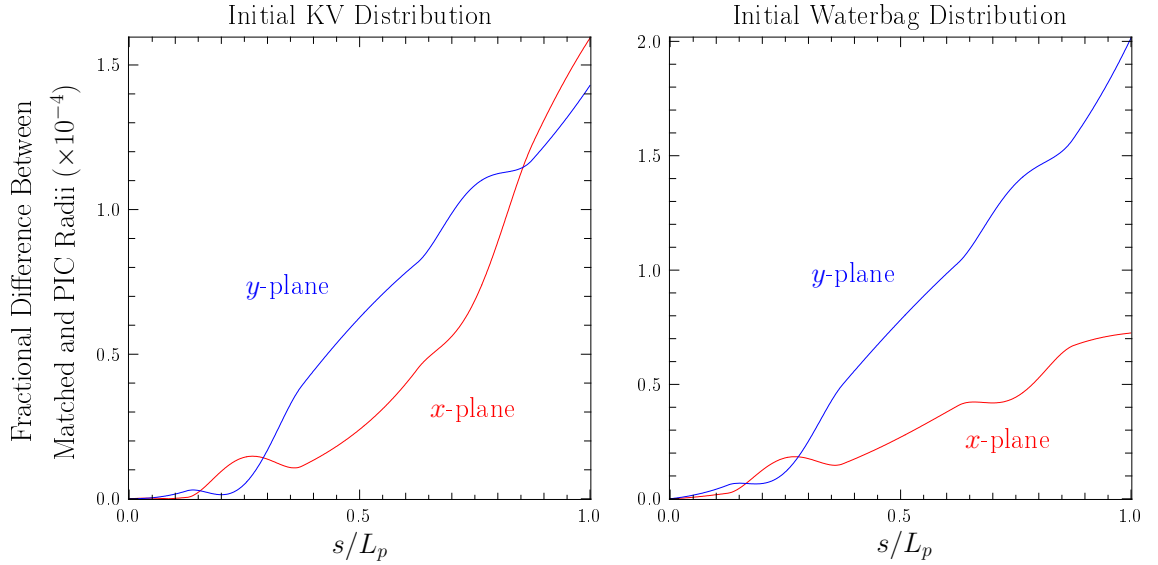| Parameters | Values |
|---|---|
| Pipe radius | 100 mm |
| Number of simulation particles | $10^6$ |
| Time steps per period | $10^3$ |
| $x$-plane grid points | 512 |
| $y$-plane grid points | 512 |
| Number of cells across beam | $\sim 50$ |
| Number of particles per grid cell | $\sim 500$ |
| Ratio of pipe radius to envelope radius | $\sim 10$ |



Figure 5.3: Fractional differences between radial solutions to the KV equations for a FODO quadrupole doublet focusing lattice (Lattice 1) and envelopes calculated from transverse slice PIC runs with the same initial conditions as the matched beam. The PIC code advances particle beams initially in the KV distribution (left) and waterbag distribution (right).
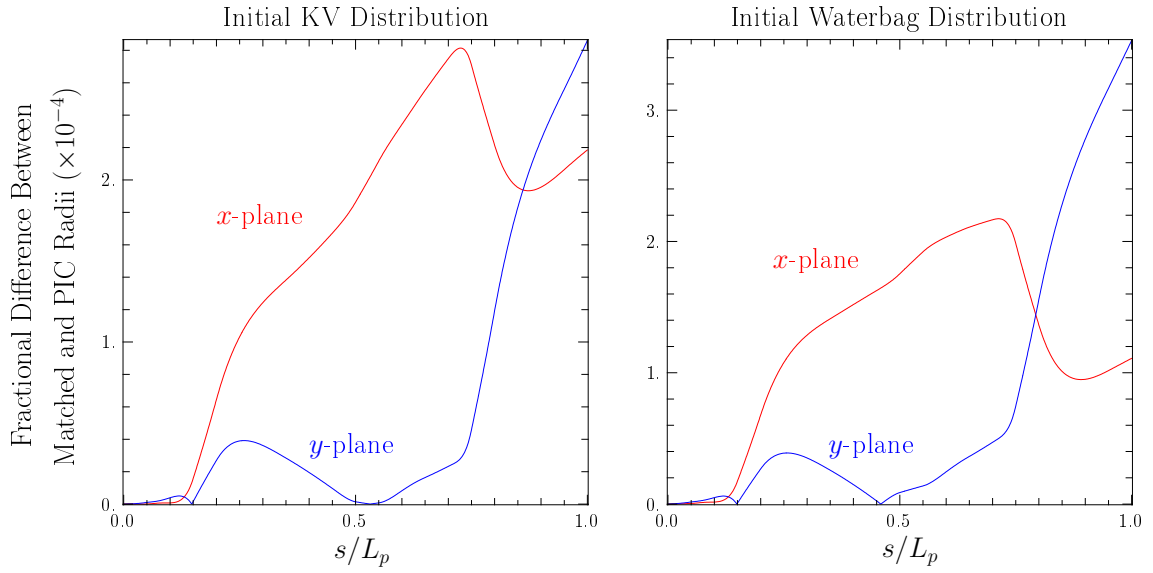
Figure 5.4: Fractional differences between radial solutions to the KV equations for a complicated quadrupole focusing lattice (Lattice 2) and envelopes calculated from transverse slice PIC runs with the same initial conditions as the matched beam. The presentation is analogous to Fig. 5.3.

# Chapter 6

# Focusing Strength Iterator

For many applications, the undpressed phase advances $\sigma_{0j}$ are calculated from the lattice focusing functions $\kappa_j$ to provide a measure of the overall lattice focusing strength. In the matching program discussed in Chapter 5, the $\sigma_{0j}$ are calculated as follows. When the lattice is read into WARP and `Match()` is called, the matching program scans the lattice focusing functions for any jump discontinuities. If any discontinuities exist, the lattice is then broken up into subdomains between the discontinuities to ensure accurate numerical integration. The matching program then solves Eq. (2.33) for the undepressed principal orbits. This is accomplished via a fixed-step RK4 scheme on each subdomain. In other words, the scheme solves Hill's Equation on the first subdomain, then uses the final condition of the first subdomain as the initial condition on the second subdomain, then solves Hill's Equation there, etc. Once the principal orbits are obtained, the undepressed phase advances are calculated from Eq. (2.34).

Conversely, if the overall shapes of the $\kappa_j$ functions are known, the lattice focusing

strengths can be specified from the $\sigma_{0j}$ given $\sigma_{0j} < 180°$. A function was written to determine the scale factor $\alpha$ by which to multiply the focusing strengths input into WARP to yield a target undepressed phase advance $\sigma_{0j}^t$. Because the focusing strengths in both transverse planes are linked, the user must specify whether the target undepressed phase advance is an $x$- or $y$-plane quantity.

The focusing strength iterator first reads in a lattice that the user has set up. The program then calculates the corresponding undepressed phase advances and computes $\sigma_{0j} - \sigma_{0j}^t$. Since we assume that both $\sigma_{0j}$ and $\sigma_{0j}^t$ are strictly positive and less than 180° for single-particle stability, a positive difference implies that $0 < \alpha < 1$, while a negative difference implies that $\alpha > 1$. In the first case, the program evaluates $\sigma_{0j} - \sigma_{0j}^t$ for decreasing values of $\alpha$ (starting with $\alpha = 1$) with a user-specificed step size $d\alpha$ (called `da` in the program) until reaching a value $\alpha = \alpha_s$ where $\sigma_{0j} - \sigma_{0j}^t < 0$. The desired $\alpha$ is then found by bisection root finding, with $\alpha_s$ and $\alpha_s + d\alpha$ as lower and upper bounds, respectively. In the second case, $\alpha$ is increased from 1 by a uniform step size until the program finds some $\alpha = \alpha_s$ where $\sigma_{0j} - \sigma_{0j}^t > 0$. The desired $\alpha$ is then found by bisection root finding, with $\alpha_s$ and $\alpha_s - d\alpha$ as upper and lower bounds, respectively.

The focusing strength iterator is contained in a script named `lattice_rescale.py`. After the lattice functions are loaded into Python (see Sec. 5.1), the focusing strength iterator may be read in with Python's `import` or `execfile` commands. A single over-arching function called `rescalefunc()` rescales the lattice focusing strength to achieve the target phase advance. This function contains the following arguments:

- `sigma0target`: real [deg/period]

Target value of depressed phase advance.

- `plane`: string

  Set to either 'x' or 'y'. Specifies `sigma0target` as an x- or y-plane quantity.

- `da`: real [1]

  Default: 0.1

  Size by which to increase or decrease the lattice strength scale from the value associated with the specified lattice to establish a bracket for root finding.

- `rftol`: real [1]

  Default: `1.e-16`

  Maximum root finding tolerance in lattice strength rescaling.

- `steps`: integer [1]

  Default: `1000`

  Number of evenly spaced intervals per lattice period to calculate particle phase advances.

- `error_stop`: logical

  Default: `True`

  If `True`, the matching program stops if any error trap is tripped and prints a message explaining the problem. If set to `False`, the program keeps running through the error, with possibly unreliable results.

  The function `rescalefunc()` has no output variables, so it is called with a command of the form

```
rescalefunc(sigma0target,plane,other inputs).
```

The variables `sigma0target` and `plane` must be specified whenever `rescalefunc()` is called, but the other input variables have default values, and thus need not be specified.

Table 6.1 lists the scale factors as calculated by `rescalefunc()` necessary to achieve the specified target phase advances for the lattices depicted in Figs. 5.3 and 5.4. Lattice 1 refers to the simple FODO lattice (Fig. 5.3), while Lattice 2 refers to the more complicated quadrupole lattice (Fig. 5.4).

Table 6.1: Scale factors necessary to achieve target phase advances

|  | Lattice 1 | Lattice 2 |
|---|---|---|
| Specified $\sigma_{0x}$ | $60°$ | $70.2307°$ |
| Target $\sigma_{0x}$ | $\alpha$ | $\alpha$ |
| $20°$ | 0.3469 | 0.3034 |
| $40°$ | 0.6836 | 0.5957 |
| $60°$ | 1 | 0.8695 |
| $80°$ | 1.2867 | 1.1173 |
| $100°$ | 1.5348 | 1.3321 |
| $120°$ | 1.7366 | 1.5072 |
| $140°$ | 1.8856 | 1.6369 |
| $160°$ | 1.9770 | 1.7166 |
| $170°$ | 2.0001 | 1.7368 |
| $175°$ | 2.0059 | 1.7419 |
| $179°$ | 2.0078 | 1.7435 |

Figure 6.1 offers a different depiction of the use of the focusing strength iterator. Given the x-plane focusing function $\kappa_x$ associated with Lattice 1, we find the principal orbit $C_{0x}$ plotted in red. A rescaled and shifted $\kappa_x$ is plotted as well for comparison. $C_{0x}$ returns to its initial conditions after 6 lattice periods, implying that the undepressed phase advance $\sigma_{0x} = 60°$. Now suppose we wish to keep the lattice elements at their same positions and relative strengths, but multiply their total strengths by some factor $\alpha$ to achieve a target undepressed phase advance $\sigma_{0x}^t = 120°$. The associated principal orbit $C_{0x}^t$ and focusing function $\alpha\kappa_x$ are plotted in blue.
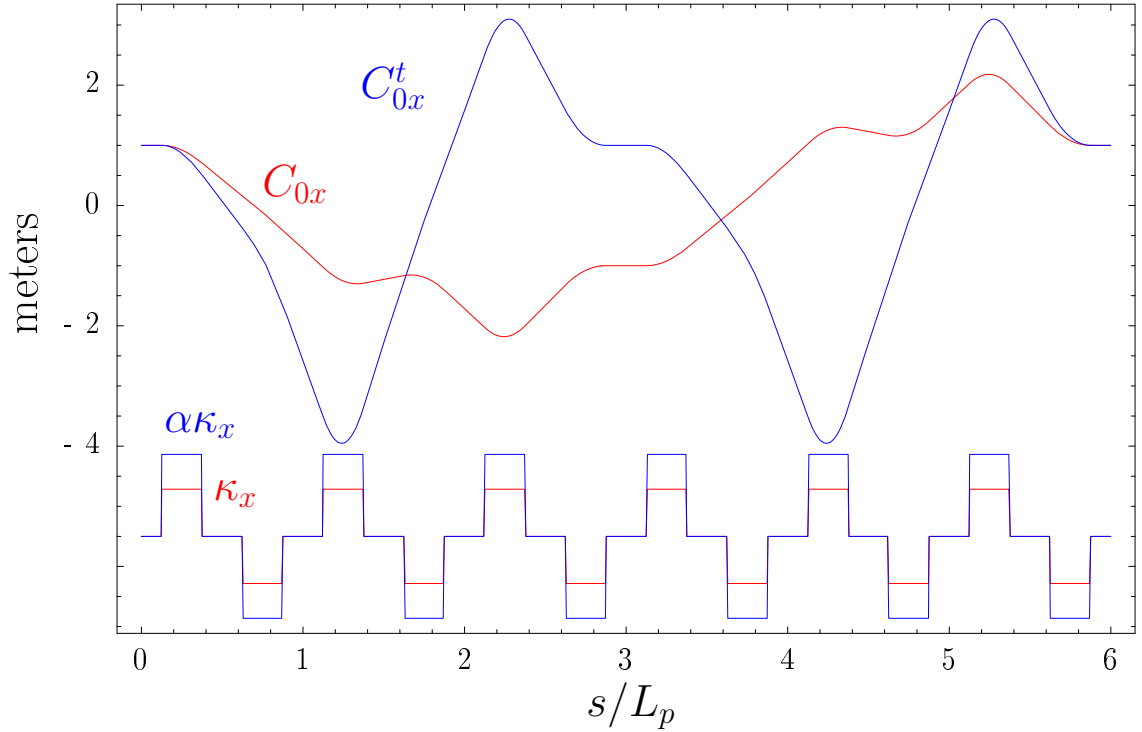


Figure 6.1: Comparison between two FODO quadrupole lattices and associated principal orbits. The initial lattice focusing function $\kappa_x$ has an undepressed phase advance $\sigma_{0x} = 60°$. $\kappa_x$ is multiplied by a scale factor $\alpha = 1.7366$ to achieve a target phase advance $\sigma_{0x}^t = 120°$. Associated principal orbits $C_{0x}$ (red) and $C_{0x}^t$ (blue) are plotted.

# Chapter 7

# Conclusion

In Ref. [6], a new iterative method for computing matched solutions to the KV envelope equations was developed. For this master's project, this iterative matching method is generalized and fully implemented in WARP, a powerful PIC code. This new incarnation of the iterative matching method can accommodate any user-specified linear applied lattice focusing function that do not exhibit skew coupling, and offers a broader set of beam parameter specification options than its predecessor. Because matched solutions to the KB envelope equations are used extensively in setting up detailed WARP simulations, the fail-safe structure and highly flexible setup of the WARP implementation should save code users considerable effort. To further enhance WARP's modeling capabilities, a Python script was added to vary the strength of a specified applied focusing lattice to achieve a target x- or y-plane undepressed phase advance.

# Bibliography

[1] W. R. Meier. Economic Systems Modeling for Laser IFE and the Potential advantages of Fast Ignition. In *European Conference on Laser Interaction with Matter, Madrid, Spain*, 2006.

[2] S. S. Yu, W. R. Meier, R. P. Abbott, J. J. Barnard, T. Brown, D. A. Callahan, C. Debonnel, P. Heitzenroeder, J. F. Latkowski, B. G. Logan, S. J. Pemberton, P. F. Peterson, D. V. Rose, G-L. Sabbi, W. M. Sharp, and D. R. Welch. An Updated Point Design for Heavy Ion Fusion. *Fusion Science and Technology*, 44:266–273, 2003.

[3] M. Reiser. *Theory and Design of Charged Particle Beams*. John Wiley & Sons, Inc., New York, 1994.

[4] R. Ryne. Finding Matched RMS Envelopes in RF Linacs: A Hamiltonian Approach. Technical Report acc-phys/9502001, http://arxiv.org, Accelerator Physics, 1995.

[5] S. M. Lund and B. Bukh. Stability Properties of the Transverse Envelope Equations Describing Intense Ion Beam Transport. *Phys. Rev. Special Topics - Accelerators and Beams*, 7:024801, 2004.

[6] S. M. Lund, S. H. Chilton, and E. P. Lee. Efficient computation of matched solutions

of the Kapchinskij-Vladimirskij envelope equations for periodic focusing lattices. *Phys. Rev. Special Topics – Accelerators and Beams*, 9:064201, 2006.

[7] H. Wiedemann. *Particle Accelerator Physics: Basic Principles and Linear Beam Dynamics.* Springer-Verlag, New York, 1993.

[8] E. D. Courant and H. S. Snyder. Theory of the Alternating-Gradient Synchrotron. *Annals of Physics*, 3:1, 1958.

[9] E. P. Lee. The Beam Envelope Equation – Systematic Solution for a Periodic Quadrupole Lattice with Space Charge. *Particle Accelerators*, 52:115, 1996.

[10] E. P. Lee. Precision Matched Solution of the Coupled Beam Envelope Equations for a Periodic Quadrupole Lattice with Space Charge. *Phys. Plasmas*, 9:4301, 2002.

[11] O. Anderson. Accurate Iterative Analysis of the K-V Equations. In *Proceedings of the 2005 Particle Accelerator Conference, Knoxville, TN*, page TPAT061. IEEE #01CH37268C, Piscataway, NJ 08855, 2005.

[12] A. Freidman, D. P. Grote, and I. Haber. Three-dimensional particle simulation of heavy-ion fusion beams. *Phys. Fluids B*, 4:2203, 1992.

[13] http://hifweb.lbl.gov/Warp/.

[14] D. P. Grote et al. WARP Manual. http://hifweb.lbl.gov/Warp/manual/manual.ps.

[15] M. Metcalf and J. K. Reid. *Fortran 90/95 Explained.* Oxford University Press, Oxford, 1999.

[16] M. Lutz and D. Ascher. *Programming Python.* O'Reilly & Associates, Inc., Sebastopol, CA, 2006.

[17] M. Lutz and D. Ascher. *Learning Python.* O'Reilly & Associates, Inc., Sebastopol, CA, 2004.

[18] http://hifweb.lbl.gov/Forthon/.

[19] J. J. Barnard. Emittance Growth from Rotated Quadrupoles in Heavy Ion Accelerators. In *Proceedings of the 1995 Particle Accelerator Conference, Dallas, TX*, page 3241. IEEE Piscataway, NJ 08855, 1995.

[20] R. A. Kishek, J. J. Barnard, and D. P. Grote. Effects of Quadrupole Rotations on the Transport of Space-Charge Dominated Beams: Theory and Simulations Comparing Linacs with Circular Machines. In *Proceedings of the 1999 Particle Accelerator Conference, New York City, NY*, page 1761. IEEE Piscataway, NJ 08855, 1999.

[21] J. J. Barnard and S. M. Lund, U.S. Particle Accelerator School courses: *Beam Physics with Intense Space-Charge*, Waltham, MA, 12 – 23 June 2006, Lawrence Livermore National Laboratory, UCRL-TM-231628 and Lawrence Berkeley National Laboratory, LBNL-62783; *Intense Beam Physics: Space-Charge, Halo, and Related Topics*, Williamsburg, Va, 19 – 20 January, 2004, Lawrence Livermore National Laboratory, UCRL-TM-203655 and Lawrence Berkeley National Laboratory, LBNL-54926; *Space-Charge Effects in Beam Transport*, Boulder, CO, 4 – 8 June, 2001, Lawrence Berkeley National Laboratory, LBNL-49286.

[22] I. Kapchinskij and V. Vladimirskij. Limitations of Proton Beam Current in a Strong

Focusing Linear Accelerator Associated with the Beam Space Charge. In *Proceedings of the International Conference on High Energy Accelerators and Instrumentation*, page 274. CERN Scientific Information Service, Geneva, 1959.

[23] R. C. Davidson. *Physics of Nonneutral Plasmas*. Addison-Wesley, Reading, MA, 1990. Re-released, World Scientific, 2001.

[24] I. Hofmann, L. J. Laslett, L. Smith, and I. Haber. Stability of the Kapchinskij-Vladimirskij (K-V) Distribution in Long Periodic Transport Systems. *Particle Accelerators*, 13:145, 1983.

[25] S. M. Lund, D. P. Grote, and R. C. Davidson. Simulations of Beam Emittance Growth from the Collective Relaxation of Space-Charge Nonuniformities. *Nuc. Instr. Meth. A*, 544:472, 2005.

[26] E.P. Lee and R. J. Briggs. The Solenoidal Transport Option: IFE Drivers, Near Term Research Facilities, and Beam Dynamics. Technical Report LBNL-40774, UC-419, Lawrence Berkeley National Laboratory, 1997.

[27] http://www.scipy.org.

[28] W. H. Press, B. P. Flannery, S. A. Teukolsky, and W. A. Vetterling. *Numerical Recipes in FORTRAN 77: The Art of Scientific Computing*. Cambridge University Press, New York, second edition edition, 1992.